Journal of Materials Chemistry A

ROYAL SOCIETY OF CHEMISTRY

REVIEW

View Article Online
View Journal | View Issue

Cite this: J. Mater. Chem. A, 2022, 10, 6351

Chemical lattice strain in nonstoichiometric oxides: an overview†

Dmitry S. Tsvetkov, *[ab] Vladimir V. Sereda, [ab] Dmitry A. Malyshkin, [ab] Ivan L. Ivanov [ab] and Andrey Yu. Zuev[a]

Strong coupling between the chemical composition and crystal lattice dimensions resulting in the contraction or expansion of a material upon change of its chemical composition is known as chemical expansion or chemical strain. This phenomenon significantly influences the performance of oxide materials in different energy conversion and storage devices. In many such applications, *e.g.*, in oxygen-permeating membranes or solid oxide fuel cells (SOFCs), the materials are subject to significant *in situ* variation of their chemical composition, which is accompanied by large volume changes. This may often be detrimental to the operation of the electrochemical device. Not only is chemo-mechanical coupling crucial for various practical applications, but also, when measured accurately and discussed appropriately, the chemical strain of an oxide material allows better understanding of its local electronic and defect structure. Chemical strain is also strongly correlated with diffusion phenomena in high-temperature electrochemical devices – the subject that for many years has been of particular scientific interest for John Kilner and where he holds a lot of pioneering achievements. This article reviews the state of the art in the field of chemical strain of various oxide materials, primarily those intended to operate at elevated temperatures, and aims at summarizing the available experimental, theoretical and computational insights into its origins, factors impacting its magnitude, and the available means for its *a priori* quantitative estimation.

Received 28th September 2021
Accepted 14th February 2022

DOI: 10.1039/d1ta08407k

rsc.li/materials-a

1. Introduction

Oxides with fluorite- and perovskite-type structures are the state-of-the-art materials for various electrochemical devices, such as solid oxide fuel cells (SOFCs),[1,2] dense oxygen-conducting membranes[3] and catalysts for various processes including those important from the ecological viewpoint, for example, oxidation of CO.[4] These oxides possess unique combinations of electrical, magnetic and catalytic properties, which can be substantially altered by engineering the chemical composition and morphology. While enhancing electrochemical performance (*e.g.* reaction rates in SOFCs) has largely been the focus in developing such energy related materials, the challenges provided by mechano-chemical and mechano-electrical coupling are becoming increasingly important for further progress in developing devices for energy conversion and storage.[5] As a result, a recently emerging field of Mechano-Electro-Chemical (MEC) coupling examining the relationships between a material's physico-electro-chemical state and its processing, structure and properties has received great attention in the last decade.[5] Mechano-chemical coupling as an important part of MEC coupling plays a crucial role, since energy-related oxide materials are commonly operated at elevated temperatures in both oxidizing and reducing environments and, upon heating, undergo not only thermal expansion, but also the one caused by a change in their oxygen content or hydration degree[6] (in case of proton-conducting oxides) or, in other words, in the concentration of point defects in them. Even the materials designed to work at low temperatures, for example, $LiMO_2$ (M = Ni, Co, Mn) based cathodes for lithium ion batteries, when subject to relatively mild thermal stresses develop inter- and intragranular cracks due to oxygen release and oxygen vacancy formation.[7–9] Therefore, understanding the origin and the microscopic mechanisms of chemical lattice strain is crucial for identifying the ways to avoid its detrimental effect on the mechanical integrity of a particular device. Moreover, chemical expansion itself, provided that its nature is well understood, may be an important source of information on the processes in solids since it is influenced by the particularities of crystal structure,[10] point defect interactions,[11–13] diffusion,[14–16] magnetic properties,[17–20] *etc.* For example, chemical expansion relaxation has been established as one of the methods for measuring diffusion and surface exchange coefficients[14–16] in oxides – topics that John Kilner has been involved in for years

[a]*Institute of Natural Sciences and Mathematics, Ural Federal University, 620002, 19 Mira St., Yekaterinburg, Russia. E-mail: dmitry.tsvetkov@urfu.ru*

[b]*Laboratory of Hydrogen Energy, Ural Federal University, 620002, 19 Mira St., Ekaterinburg, Russia*

† Electronic supplementary information (ESI) available. See DOI: 10.1039/d1ta08407k

and where he holds a lot of pioneering achievements. It is also gratifying that he was among those pioneers who showed the importance of the relationship between the host cation radius and oxygen vacancy formation for understanding the nature of chemical strain in oxides.[21] Thanks to these efforts not only chemical expansion but also oxide ion conductivity became more understandable too.

Thus, this work is aimed at giving an overview of a very important field of mechano-chemical coupling in oxide materials for energy conversion and storage taking into account various historical aspects, the state-of-the-art achievements and existing trends, inconsistencies and challenges. The review is organized as follows. First, some definitions and a selection of units for chemical expansion will be discussed. Then the current level of understanding of chemical expansion in oxides and available modeling approaches will be summarized, and some features and trends in chemical expansion of oxides of various structural types will be identified. Finally, the negative consequences and recently reported possible practical applications of chemical strain will be outlined.

The scope of any review, and this one is no exception, of course, is somehow restricted. First of all, the review is more focused on the results obtained by various experimental or computational techniques rather than on these techniques themselves. The measurement and calculation techniques will be only briefly mentioned without their thorough discussion. That is because the range of experimental and computational methods used to measure and evaluate chemical lattice strain comprises essentially all the modern techniques for investigating the composition of oxides and their dimensions on the macro-, micro- and nanoscale. The latter is not an exaggeration: in the studies of chemical expansivity, detectable changes in linear dimensions of as small as 5 pm were reported.[22] However fascinating the ever-increasing magnification of modern analytical methods, more "conventional" ones, such as thermogravimetric analysis, dilatometry, and X-ray and neutron diffraction, despite having been with us for many decades, are still indispensable when it comes to the properties of bulk materials.[23] Imaging techniques such as scanning electron microscopy[24,25] or even X-ray tomography[7] are useful for assessment of the consequences of chemical expansion, *e.g.*, the damage caused to electrochemical devices. In turn, the more complex, in terms of the experimental setups and the interpretation of the results, and more recently developed methods—transmission electron microscopy,[26] scanning probe microscopy,[27,28] X-ray absorption fine structure (EXAFS),[29] *etc.*—are well-suited for studying thin films and interfaces.[10] Various original combinations of methods, *e.g.*, Raman spectroscopy coupled with electrochemical titration[30] and time-resolved XRD coupled with potential step chronoamperometry,[31] regularly emerge, allowing previously inaccessible insights into chemical strain to be obtained. State-of-the-art computational approaches commonly employed in chemical expansion calculations are based on molecular dynamics[12,21,32] and *ab initio* density functional theory.[32–34] As seen, the great multitude of experimental and computational methods does not allow them to be reviewed in this work in detail.

Some more applied aspects of chemical expansion, such as the modeling of chemically induced stresses in membranes[35–42] and SOFCs,[43,44] were thought to be beyond the scope of this rather more fundamentally oriented review. However, our leaving them out does not mean that they are somehow unrelated – on the contrary, high quality experimental data on defect equilibria and chemical expansion of materials figure among the necessary parameters of these models.[35,36,38,43] We would also like to draw the attention of interested readers to other existing reviews[10,23,45,46] which may provide additional information on the topic.

As our review was intended for publication in the special issue in honour of Prof. John Kilner's 75th birthday, we focused it to a large extent on materials that are closer to his scientific interests – the oxides for higher-temperature applications, and there were quite a lot of those to cover. Fortunately, those important aspects of chemical strain in lithium ion conductors for low-temperature electrochemical devices that are left out of the scope of this review can be found in other recent reports.[47–52]

2. Definitions, historical aspects and choice of units

Chemical expansion is introduced by analogy with, perhaps, the most familiar type of solid body expansion – thermal expansion,[53] and these two phenomena quite often occur simultaneously. Therefore, the definitions and origins of thermal expansion should be discussed first. Indeed, it is well known that thermal expansion is a fundamental property of materials originating from asymmetry of the resulting interaction potential of site species in the crystal lattice, which leads to anharmonicity of atomic vibrations and, consequently, to an increase in the average interatomic distances with temperature. This phenomenon can be quantified using the volumetric (α_V) or linear (α_L) thermal expansion coefficients (TECs)

$$\alpha_V = \frac{1}{V_0}\left(\frac{\partial V}{\partial T}\right)_P;\ \ \alpha_L = \frac{1}{L_0}\left(\frac{\partial L}{\partial T}\right)_P, \tag{1}$$

where V_0 and L_0 are the values of volume and length in a selected initial (reference) state, and P is the total pressure. The so-called uniaxial strain is defined from dilatometric or X-ray diffraction (XRD) measurements as

$$\varepsilon_{therm} = \frac{\Delta L}{L_0} = \frac{\Delta a}{a_0} = \alpha_L \Delta T, \tag{2}$$

where ΔL and Δa are the length and the unit cell parameter increments, respectively, corresponding to the temperature change ΔT. Strictly speaking, TEC is temperature dependent as follows from the thermodynamic definition of the Grüneisen parameter:

$$\alpha_V(T) = \gamma \frac{C_V}{V_m}\chi_T, \tag{3}$$

where V_m, C_V, γ, and χ_T are the molar volume, heat capacity at constant volume, Grüneisen parameter, and isothermal compressibility, respectively.

However, the Grüneisen parameter, in the first approximation, can be treated as a temperature-independent constant for a given

substance, especially at $T \gg \Theta_D$, where Θ_D is the Debye temperature.[54] The values of χ_T and V_m for solids are also known to depend on temperature only weakly. Thus, the change in TEC with temperature is governed mainly by the temperature dependence of the specific heat. The latter is rather flat at high temperatures and therefore, $\alpha_V(T)$ tends to be a constant.[53] Therefore, if thermal expansion mostly contributes to strain then the latter can be treated as a linear function of temperature with a constant TEC.

Nevertheless, Strelkow[55] was the first who reported a significant positive deviation from the linear trend of ε with temperature for several solid halides such as NaCl, AgCl, and AgBr in the vicinity of their melting points. He called this phenomenon "abnormal expansion". Later Mott and Gurney[56] as well as Seitz[57] proposed that this anomaly in expansion should be attributed to point defects arising in the crystal lattice at elevated temperatures. Indeed, Lawson[58] compared the activation heat for abnormal expansion to that determined earlier for ionic conductivity of silver halides, found good agreement between both values, and concluded that the "abnormal expansion" is caused by the increasing concentration of lattice defects responsible for the ionic conductivity. Using ionic radii Lawson[58] also first calculated the volume expansion caused by Schottky defect formation and found the calculated values to be completely consistent with those reported by Strelkow.[55]

Thus, "abnormal expansion" of the crystal lattice originates from the points defect formation therein and depends on the concentration of defects. Hence, such expansion can be observed at a constant temperature – for example, when the content of the volatile component in the gas phase changes. For this reason, it is also called "isothermal," "defect-induced," or "chemical" expansion, to emphasize the difference between its nature and the usual thermal expansion.

Surprisingly, the first evidence that oxides can exhibit chemical expansion appeared prior to Strelkow's pioneering work. Back in 1933, the volume of the unit cell of wustite, $Fe_{1-y}O$, was found[59] to depend on the content of iron vacancies, which can indicate the change of iron cation radius upon its reduction or oxidation. Nevertheless, extensive study of the isothermal expansion of oxides began only in the 90s of the 20th century because of their wide application as energy-related materials. To date, a lot of evidence has been reported in the literature to demonstrate that the phenomenon of chemical expansion is inherent in many such complex oxide materials.[10]

In broad terms, chemical strain or chemical expansion of solids can be defined as the change in their dimensions following any change in their composition. Even the host/dopant cation concentration ratio, which is set during the synthesis and then remains fixed, can play the role of the composition parameter. Then, electrochemical processes can be used to change the cationic composition of oxides. Lithiation/delithiation occurring in Li-ion battery cathodes is, perhaps, among the most prominent examples of this.[52,60] Finally, if a material is redox active or hydratable, its chemical composition may, of course, vary *in situ* at sufficiently high temperature upon equilibration with the surrounding atmosphere.

Fig. 1 outlines a few reasons behind the chemical lattice strain of oxides—substitution, redox processes and hydration—on which this review is focused. While Fig. 1 provides a useful visual metaphor, the real physical processes underlying chemical expansion can be much more complex. For instance, in Fig. 1 the sample preserves its phase state during the chemical composition change. Marrocchelli *et al.*[61] suggested to call this type of chemical expansion "stoichiometric" in contrast to "phase change expansion" when the sample's phase state is changing as well. The former represents the main subject of the current review.

The use of TEC only is, therefore, insufficient for a full definition of solid oxides' expansion when substantial amounts of defects form at elevated temperatures. For example, in the case of the oxygen-nonstoichiometric oxide, the overall lattice strain can be quantified in terms of both usual volumetric TEC (α_V) and volumetric chemical expansivity (α_{VC}) induced by oxygen vacancy formation as suggested by Adler[62]

$$\alpha_{VC} = \frac{1}{V_0}\left(\frac{\partial V}{\partial X_{V_O}}\right)_{T,P}, \quad (4)$$

where X_{V_O} is the oxygen vacancy mole fraction, and V_0 is the specific volume of an oxygen-stoichiometric composition at a given temperature. The former quantity is defined, for example, as $\delta/3$ for $ABO_{3-\delta}$ perovskite oxides, where δ is the oxygen nonstoichiometry. Using the aforementioned definitions, the total derivative of the uniaxial strain ε in the absence of additional pressure or mechanical forces can be given[62] as

$$d\varepsilon(T, X_{V_O}) = \frac{1}{3}\alpha_V dT + \frac{1}{3}\alpha_{VC} dX_{V_O}. \quad (5)$$

Eqn (5), valid for isotropic materials, enables simultaneous determination of both thermal and chemical constituents of the

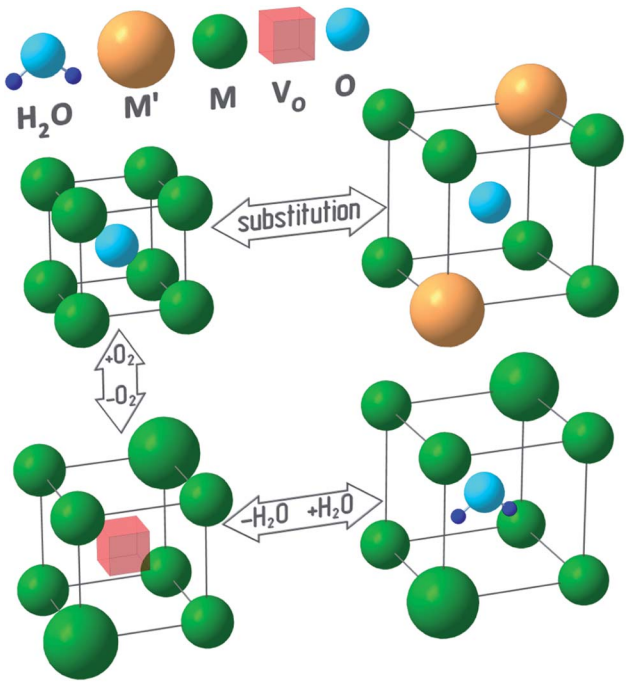

Fig. 1 Possible causes of chemical expansion of oxide materials, represented for a hypothetical $M_{1-x}M'_xO_{1-y}(H_2O)_z$ oxide.

uniaxial isotropic strain, for instance, of cubic oxides measured at a given oxygen partial pressure (p_{O_2}) depending on temperature. However, such a thermodynamic approach, firstly, is not applicable for layered oxides exhibiting anisotropic chemical strain and, secondly, it does not allow the origin of chemical strain itself to be understood.

Eqn (4) describes only one possible definition of chemical expansivity.[61] Depending on how the concentration of the defects responsible for chemical strain is defined, at least three possibilities exist:

(1) the concentration may be defined as a molar fraction of defects in the corresponding sublattice, *i.e.* $X_{V_O} = \frac{\delta}{3}$ in the case of $ABO_{3-\delta}$ oxide. This is similar to eqn (4). Hence, the uniaxial expansivity is

$$\beta_X = \frac{1}{L_0}\left(\frac{\partial L}{\partial X_{V_O}}\right)_{T,P}; \quad (6)$$

(2) if the concentration is defined in cm^{-3}, then the chemical expansion coefficient is

$$\beta_{C_V} = \frac{1}{L_0}\left(\frac{\partial L}{\partial C_{V_O}}\right)_{T,P}, \quad (7)$$

where C_{V_O} is concentration in cm^{-3}, and the coefficient β_{C_V} has units of volume (cm^3);

(3) if the concentration is defined in moles per mole of oxide (for example, $ABO_{3-\delta}$), then the chemical expansivity is

$$\beta = \frac{1}{L_0}\left(\frac{\partial L}{\partial \delta}\right)_{T,P} \quad (8)$$

and the coefficient β is dimensionless.

Although it may be argued[61] that β_X and β_{C_V} should be preferred for the comparison among different structural types, it is the β-coefficient which is the most used in current practice for convenience reasons. This way of expressing chemical expansivity will be used throughout this review.

In the case of proton conducting oxides exhibiting chemical expansion upon hydration,[6] a similar definition of expansivity will be employed. In addition, the amount of water, x, per mole of hydrated oxide, $ABO_{3-\delta-x}\cdot xH_2O$, is used as a composition variable[34,63,64] instead of the concentration of protons in the crystal structure employed in ref. 65–70 so that β would reflect the expansion per mole of hydrated oxygen vacancies:

$$\beta = \frac{1}{L_0}\left(\frac{\partial L}{\partial x}\right)_{T,P}, \quad (9)$$

where x is the number of moles of water per mole of oxide.

3. Various models and approaches to understand the chemical expansion

3.1. Fluorites

The pioneering targeted studies of chemical expansion in oxide materials concerned primarily the oxides with a fluorite-like structure. These studies were aimed at finding the compositional dependences of unit cell dimensions for MO_2–R_2O_3 and MO_2–ZO (M = Hf, Zr, Ce, Th, U; R = Y, Gd, Yb, Zr, Sc, La, Sm, Eu; Z = Ca, Mg, Sr) solid solutions. Cubic symmetry, typical of the fluorite crystal structure, was found to be retained upon MO_2–R_2O_3 and MO_2–ZO substitutions for all solid solutions up to the respective solubility limits.[71]

Based on the geometrical considerations an expression for the unit cell parameter can be derived:[72]

$$a = \frac{4}{\sqrt{3}}(r_M + r_O), \quad (10)$$

where r_M and r_O are the radii of M^{4+} (coordination number (CN) = 8) and O^{2-} (CN = 4), respectively. However, eqn (10) is not applicable to complex fluorite oxides formed by aliovalent substitution, because, in addition to the cation radius change, oxygen vacancies form in the crystal structure upon such substitution, *e.g.* according to the following defect reaction (written using the Kröger–Vink notation employed hereafter):

$$R_2O_3 \xrightarrow{MO_2} 2R'_M + 3O_O^{\times} + V_O^{\cdot\cdot}, \quad (11)$$

which may also influence the unit cell dimensions.

To take this into account Glushkova *et al.*[73] suggested modifying the ionic radii in eqn (10), replacing r_M with a weighted mean ionic radius, $xr(R^{3+}) + (1-x)r(M^{4+})$, and r_O with an "effective" oxygen ion radius, r_{eff}. In this approach, the oxygen vacancy is thought to occupy no space. Hence, the effective oxygen ion volume is equal to $4/3\cdot\pi {r_O}^3\cdot(1-x/4)$, and $r_{eff} = r_O(1-x/4)^{1/k}$, where $k = 3$ for noninteracting vacancies and $k > 3$ for cases when oxygen vacancies form clusters.[73] In the original work, the value of $k = 3.6$ was used for calculating the unit cell parameter a.

Ingel and Lewis,[74] applying the model suggested by Aleksandrov *et al.*[75] for calculating the unit cell parameters of yttrium-stabilized zirconia (YSZ) as a function of Y content, arrived at the following equation:

$$a = \frac{4}{\sqrt{3}}\left(r_{Zr} + r_O + \frac{2x(r_Y - r_{Zr})}{100 + x}\right), \quad (12)$$

where r_Y, r_{Zr}, r_O and x are the radii of Y^{3+}, Zr^{4+}, and O^{2-}, and the molar fraction of Y_2O_3 (in percent), respectively.

The aforementioned models work well for those solid solutions for which they were initially derived, and when applied to different materials give significant discrepancies between the calculated and experimental data.[76,77] The later efforts were directed at finding more general models.

According to the empirical Vegard's rule,[78] the relationship between the unit cell parameters and concentrations of the solid solution components should be linear. We should mention here that, being simple as well as very general, Vegard's rule plays an important role in the analysis of chemical strain in some cases, *e.g.*, in thin films of Li ion conductors. Therein, terms such as "Vegard strain" or "Vegard coefficient" are sometimes used to describe chemical strain that linearly depends on the concentration of ions or the slope of such dependence.[79,80] However, chemical expansion as a bulk property of highly nonstoichiometric oxides often deviates from

a simple linear compositional dependence predicted with Vegard's rule.

Assuming that oxides MO_2 (M = Hf, Zr, Ce, Th, U) with a fluorite structure conform to Vegard's rule, Kim[76] developed a model that is also, by its nature, empirical. For example, an expression for the unit cell parameter a of the substituted ceria in Kim's model framework is

$$a = 0.5413 + \sum_i (0.0220(r_i - r_{Ce}) + 0.00015(z_i - z_{Ce}))m_k, \quad (13)$$

where r_i and z_i are the radius (in nm) and the valence of the ith cation, r_{Ce} and z_{Ce} are the radius and the valence of Ce ions, and m_k is the molar fraction of MO_x in the CeO_2–MO_x solution.

Discussing the fact that the oxygen vacancy located near M^{4+} in MO_{2-x} can effectively lower the coordination number of the cation, Hong and Virkar[72] suggested a model for calculating a of variously substituted ceria and zirconia. In place of variable CN, they introduced another parameter – oxygen vacancy radius r_V, independent of the concentration and nature of the dopant. As a result, the value of a can be obtained by replacing r_M and r_O in eqn (10) with the weighted mean cation and anion radii, respectively:

$$a = \frac{4}{\sqrt{3}}(xr_R + (1-x)r_{Ce} + (1-0.25x)r_O + 0.25xr_V)0.9971, \quad (14)$$

where x is the dopant (R) molar fraction, and r_R, r_{Ce}, r_O, and r_V are the R^{3+} (R = Yb, Er, Ho, Dy, Gd, Sm, Nd, La), Ce^{4+}, O^{2-} and $V_O^{\cdot\cdot}$ radii, respectively. The 0.9971 multiplier is added to make the calculated a parameter of undoped CeO_2 equal to the experimental one (5.411 Å).

The values of r_V were found using the experimental $\partial a/\partial x = f(r_R)$ plots. From them, the critical cation radii r_R^* were determined, which are hypothetical r_R at which substituting R for Ce in CeO_2 (or Zr in ZrO_2) does not change a, *i.e.* $\partial a/\partial x = f(r_R^*) = 0$. Next, substituting r_R^* into $\partial a/\partial x = 0$ with a as per eqn (14) yielded the following expression:

$$r_R^* + r_{Ce} - 0.25r_O + 0.25r_V = 0. \quad (15)$$

The as-calculated r_V was found to be 1.164 Å for $RO_{1.5}$–CeO_2 and 0.993 Å for $RO_{1.5}$–ZrO_2, as compared with the ionic radius of O^{2-} (1.38 Å).

Thus, as follows from eqn (14) and (15), the total chemical expansion observed upon changing the composition of fluorite-type oxides is due to the simultaneous unit cell expansion, caused by the cation size increase, and contraction, caused by the formation of oxygen vacancies that are smaller than oxygen ions. For example, the experimentally determined chemical expansion of $CeO_{2-\delta}$, which can be thought of as a solid solution of Ce_2O_3 in CeO_2, is $\Delta a/a_0 \approx 10\%$ per mole of oxygen vacancies, which in the framework of the model of Hong and Virkar[72] is a result of ≈15% "cationic" expansion and ≈5% oxygen-vacancy-induced contraction.[45]

Similarly to eqn (14), Marrocchelli *et al.*[12] expressed an equation for the relative elongation of $R_xM_{1-x}O_{2-x/2}$ (M = Zr, Ce; R = Y, Yb, Ho, Er, Dy, Gd, Nd, Sm, Tb, La, Pr, Ce):

$$\frac{a-a_0}{a_0} = \frac{(r_{cation} + r_{anion}) - (r_M + r_O)}{r_M + r_O} = \left[\frac{r_R - r_M}{r_M + r_O} + \frac{1}{4}\frac{r_V - r_O}{r_M + r_O}\right]x = (\beta_M + \beta_V)x = \beta x, \quad (16)$$

where x is the molar fraction of the R cation, r_R, r_M, r_V, and r_O are the radii of R^{3+}, M^{4+}, O^{2-}, and $V_O^{\cdot\cdot}$, and $\beta_M = (r_R - r_M)/(r_M + r_O)$ and $\beta_V = (r_V - r_O)/4(r_M + r_O)$ are the "partial" chemical expansion coefficients, reflecting the magnitude of expansion arising from the cation radius change and vacancy formation, respectively. As $\beta_M + \beta_V = \beta$, the oxygen vacancy radius is equal to:

$$r_V = 4(r_M + r_O)(\beta - \beta_M) + r_O, \quad (17)$$

where, if Shannon ionic radii[81] are used to calculate β_M, the only unknown value in the right-hand side is β. In the work of Marrocchelli *et al.*,[12] β for $R_xM_{1-x}O_{2-x/2}$ was determined by three different methods: from the (a) experimental data, taken from the literature, (b) molecular dynamics (MD) simulations and (c) *ab initio* density functional theory (DFT) calculations. The as-obtained r_V values, presented in Table 1, are relatively close to each other. A more detailed discussion of DFT and MD is given below.

It has to be noted that r_V should not be considered as the real size of oxygen vacancies. The so-called vacancy radius is rather a certain effective value reflecting the local crystal lattice size changes following the $V_O^{\cdot\cdot}$ formation.[71]

The aforementioned $a(M_{1-x}R_xO_{2-\delta}) = f(r_i, x, \ldots)$ model dependences were derived primarily using the room-temperature XRD data for different series of solid solutions where both oxygen nonstoichiometry and cationic composition varied. However, the chemical expansion occurring at elevated temperatures for oxides with varying oxygen nonstoichiometry (upon p_{O_2} changes) is no less important. This is evidenced by a number of studies devoted to this phenomenon for doped and undoped ceria.[11,12,21,82–91]

As mentioned above, partially reduced $CeO_{2-\delta}$ can be seen as a solution of Ce_2O_3 in CeO_2,[82] which allows models such as Kim's[76] or Hong and Virkar's[72] to be applied to this oxide expansion. Being based on Vegard's rule, these models assume by definition that chemical strain *vs.* nonstoichiometry dependences are linear. The actual $\varepsilon_{chem} = f(\delta)$ dependences, however, are nonlinear for $CeO_{2-\delta}$ (ref. 82 and 92) and $Ce_{1-x}Gd_xO_{2-\delta}$,[84,93,94] especially at large deviations from stoichiometry ($\delta > 0.06$ (ref. 94) for $Ce_{0.9}Gd_{0.1}O_{2-\delta}$ and $\delta > 0.1$ for $CeO_{2-\delta}$ (ref. 92)).

Table 1 Oxygen vacancy radii in partially substituted fluorite oxides[12,72,77]

MO_2	CeO_2					ZrO_2		
Method[a]	EXP[77]	EXP[72]	MD[12]	DFT[12]	EXP[12]	EXP[12]	MD[12]	EXP[72]
r_V, Å	1.123	1.164	1.07	1.07	1.169	0.988	1.02	0.993

[a] EXP – experimental, MD – molecular dynamics simulation, DFT – density functional theory.

One likely hypothesis explaining the nonlinearity of $\varepsilon_{chem}(\delta)$ considered it to be caused by formation of electrostatic clusters, such as $(Ce'_{Ce}V^{\cdot\cdot}_{O}Ce'_{Ce})^{\times}$,[84,94–96] and oxygen vacancy ordering at high δ.[11,94] This was made use of by Bishop *et al.*[84,94] who suggested a defect chemistry based approach to discussing the chemical expansion of doped ceria. Indeed, the defect structure modeling results showed that one oxygen exchange reaction,

$$2Ce^{\times}_{Ce} + O^{\times}_{O} \rightleftarrows V^{\cdot\cdot}_{O} + 2Ce'_{Ce} + \frac{1}{2}O_2, \quad (18)$$

is not enough to describe the oxygen nonstoichiometry of ceria oxides, and adding the point defect association reactions such as

$$Ce'_{Ce} + V^{\cdot\cdot}_{O} \rightleftarrows \left(Ce'_{Ce}V^{\cdot\cdot}_{O}\right)^{\cdot}, \quad (19)$$

$$2Ce'_{Ce} + V^{\cdot\cdot}_{O} \rightleftarrows \left(Ce'_{Ce}V^{\cdot\cdot}_{O}Ce'_{Ce}\right)^{\times}, \quad (20)$$

$$2\left(Ce'_{Ce}V^{\cdot\cdot}_{O}Ce'_{Ce}\right)^{\times} \rightleftarrows \left(4Ce'_{Ce}2V^{\cdot\cdot}_{O}\right)^{\times}, \quad (21)$$

to the model improves the quality of fit. As the model $(Ce'_{Ce}V^{\cdot\cdot}_{O})^{\cdot}$ concentration was found to be low,[84] it was assumed that oxygen vacancies form clusters predominantly in accordance with eqn (20) and eqn (21),[83,84,94] the latter process describing the experimentally determined $V^{\cdot\cdot}_{O}$ ordering along the ⟨111⟩ directions in the crystal lattice of ceria at high δ.[11] Supposing the size of $(Ce'_{Ce}V^{\cdot\cdot}_{O}Ce'_{Ce})^{\times}$ or $(4Ce'_{Ce}2V^{\cdot\cdot}_{O})^{\times}$ to be different from the sum of the individual point defect sizes, Bishop *et al.*[84,94] concluded that these clusters' contributions to chemical expansion should also be different, which can be expressed as

$$\frac{\Delta a}{a_0} = \left[\beta_0(1 - X_1 - X_2) + \beta_1 X_1 + \frac{1}{2}\beta_2 X_2\right]\Delta\delta, \quad (22)$$

where X_1 and X_2 are the fractions of $(Ce'_{Ce}V^{\cdot\cdot}_{O}Ce'_{Ce})^{\times}$ and $(4Ce'_{Ce}2V^{\cdot\cdot}_{O})^{\times}$, and β_0, β_1, and β_2 are the chemical expansion coefficients due to $V^{\cdot\cdot}_{O}$, $(Ce'_{Ce}V^{\cdot\cdot}_{O}Ce'_{Ce})^{\times}$ and $(4Ce'_{Ce}2V^{\cdot\cdot}_{O})^{\times}$ formation, respectively. For calculating X_1 and X_2, defect structure models based on eqn (18) and (20) for $CeO_{2-\delta}$ (X_2 was taken as 0)[84] and eqn (18), (20) and (21) for $Ce_{0.9}Gd_{0.1}O_{2-\delta}$ (ref. 94) were used. The β_0, β_1, and β_2 coefficients were determined by fitting.

Fig. 2 shows the experimental data and model functions for chemical strain of $CeO_{2-\delta}$ and $Ce_{0.9}Gd_{0.1}O_{2-\delta}$.[84,92,94]

It is seen that Kim's[76] and Bishop's[84] models (eqn (13) and (22), respectively) agree much better with experimental data for $CeO_{2-\delta}$, while for $Ce_{0.9}Gd_{0.1}O_{2-\delta}$ even eqn (22) where oxygen vacancy ordering is taken into account does not describe the experimental ε_{chem} within the whole nonstoichiometry range.

In this respect it should be noted that the real microscopic picture of ceria solid solutions on the local scale may be much more complex than that assumed by Bishop *et al.*[84] in his analysis as shown recently in the excellent studies of Artini *et al.*[97–104] They found that the clusterization of a rare-earth dopant with oxygen vacancies leads to the formation of microheterogeneity which at some point results in crystallization of the $Ia\bar{3}$ cubic C-phase, typical of sesquioxides of the rare earths from Gd to Lu, where the latter are six-coordinated by oxygen. For larger rare-earth dopant-cations formation of a hybrid H-phase intermediate between the fluorite (F) and C phases was observed, where the F-based solid solution mainly hosts randomly dispersed C clusters. These C-type microdomains are so intimately mixed with the matrix F-phase that diffraction peaks common to the F and C phases are perfectly superimposed, and the C cell size is exactly doubled with respect to that of the F-phase. Importantly, local probes such as Raman spectroscopy, selected area electron diffraction (SAED), transmission electron microscopy (TEM), extended X-ray absorption fine structure (EXAFS) and some others unambiguously show that a certain number of C-based nano- or microdomains remain stable within the F-matrix even within the fluorite stability region irrespective of the nature of rare-earth dopant cations. What is more, the real distribution of dopant between F and C phases remains unknown. All these circumstances cast doubt on the results of geometrical interpretations of chemical lattice strain described above, and the problem should be

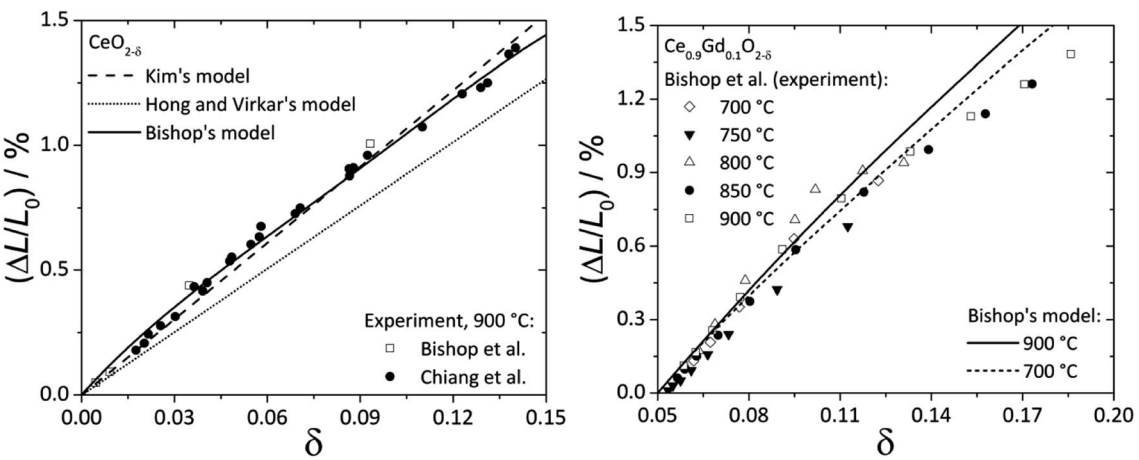

Fig. 2 Chemical expansion of $CeO_{2-\delta}$ (ref. 84 and 92) (left) and $Ce_{0.9}Gd_{0.1}O_{2-\delta}$ (ref. 94) (right): points – experiment, lines – calculations according to Kim's,[76] Bishop's[84] or Hong and Virkar's[72] model.

reexamined taking into account the new data on the local structure of ceria solid solutions.[97–104]

3.2. Perovskites

3.2.1. Reduction-induced lattice expansion. In contrast to ceria and zirconia based oxides, for perovskite-like ones chemical expansion phenomena were investigated predominantly depending on the oxygen nonstoichiometry and not the cationic composition.

The unit cell parameter a of an ideal cubic perovskite, ABO_3, may be expressed as

$$\begin{cases} a = \sqrt{2}(r_A + r_O) \\ a = 2(r_B + r_O) \end{cases}, \quad (23)$$

where r_A, r_B, and r_O are the radii of the corresponding ions. Strictly speaking, eqn (23) is applicable to a very small fraction of the vast family of perovskite oxides due to the geometric distortions of their crystal lattice, caused by variations of r_A and r_B, deviations from stoichiometry or Jahn–Teller effects.[105,106] However, the pseudocubic unit cell parameter a is often used for comparison between different perovskites possessing cubic symmetry and rhombohedral or even orthorhombic distortions. In fact, very few articles deal with anisotropic chemical expansion of perovskites,[107–110] most of the studies being focused on the isotropic chemical strain $\varepsilon_{chem} = (\Delta L/L_0)_{T=const} = \frac{1}{3}(\Delta V/V_0)_{T=const}$ of the pseudocubic lattice.

A number of chemical expansion models for fluorites are based on eqn (10). Likewise, one of the geometric models relating the ionic radii with chemical expansion[32,111,112] was inspired by the empirical approach to perovskite unit cell parameter calculations[113] based on eqn (23). In this model, first applied to substituted lanthanum gallates,[32,111] parameters A, B and C are introduced,

$$a = \frac{A}{\sqrt{2}}(r_A + r_O) + B(r_B + r_O) + C, \quad (24)$$

to account for the fact that for real, distorted perovskites the values of a calculated directly with the first and second expressions in eqn (23) would differ from each other. By fitting eqn (24) to experimentally determined a data for 77 stoichiometric ABO_3 oxides, the following values were obtained: $A = 0.816$, $B = 1.437$ and $C = -0.609$.[32] The fact that $B > A$ indicates that r_B influences a (hence, chemical expansion) to a greater degree than r_A, which was also observed in experiments.[114,115]

Change of the oxygen nonstoichiometry of a perovskite that occurs simultaneously with cation reduction/oxidation can be written as a transition from some initial state $A^0B^0O^0_{3-\delta}$ to the final one, $A^0_{1-x}A^1_xB^0_{1-y}B^1_yO^1_{3-\delta}$. For example, for lanthanum gallate $La_{1-x}Sr_xGa_{1-z}Ni_zO_{3-\delta}$ the final state is written in the $A^0_{1-x}A^1_xB^0_{1-y}B^1_yO^1_{3-\delta}$ form as

$$La_{1-x}{}^{3+}Sr_x{}^{2+}\left(Ga_{1-z}{}^{3+}Ni_z{}^{3+}\right)_{1-y}\left(Ga_{1-z}{}^{3+}Ni_z{}^{2+}\right)_yO_{3-\frac{x+yz}{2}}. \quad (25)$$

The indices x, y, and z from eqn (25) are used for deriving the expression for chemical deformation of oxides:

$$\begin{cases} \varepsilon_{chem} = \dfrac{a - a_0}{a_0} = \beta_A(x - x_0) + \beta_B(y - y_0) + \beta_V\dfrac{(x - x_0 + z(y - y_0))}{2} \\ \beta_V = \dfrac{1}{3}\left(\dfrac{A}{\sqrt{2}} + B\right)\dfrac{r_V - r_O}{a_0} \end{cases}, \quad (26)$$

where β_A, β_B, and β_V are the coefficients of chemical expansion due to the A-cation, B-cation, and oxygen vacancy formation, respectively, a_0 is the unit cell parameter in the reference state, and r_V and r_O are the oxygen vacancy and oxygen ion radii. If the chemical expansion upon A-site substitution is considered, $A^0 \neq A^1$ and $B^0 = B^1$, and the experimentally determined chemical expansion coefficient β is calculated as

$$\begin{cases} \beta_A = \dfrac{A}{\sqrt{2}}\dfrac{r_{A^1} - r_{A^0}}{a_0} \\ \beta_B = 0 \\ \beta = \beta_V + 2\beta_A \end{cases}. \quad (27)$$

In case of B-sublattice cation change (as a result of substitution or redox processes), $A^0 = A^1$ and $B^0 \neq B^1$, and

$$\begin{cases} \beta_A = 0 \\ \beta_B = B\dfrac{r_{B^1} - r_{B^0}}{a_0} \\ \beta = \beta_V + \dfrac{2}{z}\beta_B \end{cases}. \quad (28)$$

The detailed derivation of eqn (27) and (28) from eqn (26) is given in ref. 32. Among the several parameters in this model, A, B and C coefficients are pre-determined, β_A and β_B are calculated using Shannon ionic radii,[81] and β can be found experimentally, so the only unknown parameter left is the oxygen vacancy radius r_V. Interestingly, for a number of different oxides ($La_{1-x}Sr_xGa_{1-y}Mg_yO_{3-\delta}$, $La_{1-x}Sr_xAlO_{3-\delta}$, $SrTi_{1-x}Ga_xO_{3-\delta}$, $La_{0.9}Sr_{0.1}Ga_{1-x}Ni_xO_{3-\delta}$, and $SrTi_{0.65}Fe_{0.35}O_{3-\delta}$) the r_V parameter calculated using both experimental and computational expansion data and eqn (26)–(28) was in the range of 1.24–1.57 Å,[32,112] which is much closer to r_O than r_V in fluorites computed using similar geometric models.[12,72] However, no apparent relationship was found between r_V and the perovskite-like complex

oxide composition,[32] which severely limits the predictive power of such a model. This is, in principle, a common drawback of all the models based solely on the geometrical considerations and containing a number of variable coefficients to be determined by fitting and at the same time lacking the connection to the defect chemistry of oxides.

A similar approach, based on eqn (23), was developed for describing the chemical expansion of $La_{1-x}Sr_xGa_{1-y}Mg_yO_{3-\delta}$ by Chatzichristodoulou *et al.*[71] Its major differences from the one described above are two, instead of three in eqn (24), empirical fitting parameters, p_1 and p_2:

$$a = \frac{p_1}{\sqrt{2}}(r_A + r_{anion}) + p_2(r_B + r_{anion}), \quad (29)$$

where for $A^0_{1-x}A^1_xB^0_{1-y}B^1_yO_{3-0.5x-0.5y}$ with the valence difference between A^0 and A^1 or between B^0 and B^1 equal to 1, $r_{anion} = r_O(3 - 0.5x - 0.5y) + r_V(0.5x + 0.5y)/3$. Regarding the oxygen vacancy size r_V, the conclusions of Marrocchelli *et al.*[32] and Chatzichristodoulou *et al.*[71] concur: the latter found that the difference between r_V and r_O is much less noticeable in perovskites such as doped lanthanum gallates than in fluorite oxides (≈6% and ≈13–37%, respectively[71]).

Another geometry-based approach to chemical expansion modeling is also built upon the concept of ionic radii. However, in this case an attempt is made to account for the defect chemistry of an oxide. Therein, no intermediate calculations of unit cell parameters are attempted, and the radii are used in a more straightforward way. For instance, Miyoshi *et al.*[116] suggested that, as chemical expansion of $LaMnO_{3-\delta}$ should be due to Mn ions changing their size with their oxidation state, a following equation could be used for calculating the chemical strain:

$$\varepsilon_{chem} = \frac{2\Delta\bar{r}_{Mn}}{a_0} = \frac{2\left(r_{Mn^{2+}}\left[Mn'_{Mn}\right] + r_{Mn^{3+}}\left[Mn^{\times}_{Mn}\right] + r_{Mn^{4+}}\left[Mn^{\bullet}_{Mn}\right] - r_{Mn^{3+}}\right)}{a_0}, \quad (30)$$

where a_0 and $\Delta\bar{r}_{Mn}$ are the unit cell parameter of stoichiometric $LaMnO_3$ and the difference between the mean weighted radius of Mn^{n+} and Mn^{3+}, respectively. The point defect concentrations, $[Mn'_{Mn}]$, $[Mn^{\times}_{Mn}]$ and $[Mn^{\bullet}_{Mn}]$, were found using the corresponding defect structure model.[117] Similar to the expression in eqn (30), an equation

$$\varepsilon_{chem} = \frac{2\Delta\bar{r}_B}{a_0} = \frac{2\left(r_{B^{3+}}\left[B^{\times}_B\right] - r_{B^{4+}}\left[B^{\bullet}_B\right]\right)}{a_0} = \frac{4(r_{B^{3+}} - r_{B^{4+}})}{a_0}\delta, \quad (31)$$

where B is the Cr or Co ion, was used for estimating the chemical expansion of A-site-substituted lanthanum chromites[116] and cobaltites.[118] While for $LaMnO_{3-\delta}$ at some temperatures (600–700 °C) the calculated and experimental $\varepsilon_{chem}(\delta)$ dependences agreed with each other, for $La_{1-x}M_xCrO_{3-\delta}$ (M = Sr, Ca) and $La_{0.8}Sr_{0.2}CoO_{3-\delta}$ as well as at higher T (900–1000 °C) for $LaMnO_{3-\delta}$ the calculated ε_{chem} values were overestimated. The authors[116,118] attributed this discrepancy to the crystal lattice distortions causing contraction of the pseudocubic unit cell upon oxygen vacancy formation.

Zuev *et al.*[119] and Hilpert *et al.*[120] pointed out a similar behavior of $\varepsilon_{chem} = \Delta L/L_0$ and $\Delta r_B/r^0_B$, which is the relative change of the mean weighted radius of the B cation in ABO_3, with both p_{O_2} and δ for a number of promising SOFC interconnect materials – lanthanum chromite perovskites: $La_{1-x}Ca_xCrO_{3-\delta}$ ($x = 0.1$, 0.2), $La_{0.8}Sr_{0.2}CrO_{3-\delta}$, $La_{0.8}Sr_{0.2}Cr_{0.97}V_{0.03}O_{3-\delta}$, $La_{0.95}Ca_{0.05}Cr_{0.84}Al_{0.16}O_{3-\delta}$, $LaCr_{0.79}Co_{0.05}Al_{0.16}O_{3-\delta}$, and $LaCr_{0.79}Mg_{0.05}Al_{0.16}O_{3-\delta}$. Examples of such dependences are shown in Fig. 3 and 4. The appropriate defect structure models[119,120] were used to calculate the B-site point defect concentrations under the different conditions needed to evaluate Δr_B.

In principle, Co^{2+} ions can exist in low- (LS) and high-spin (HS) states. Among two possible $\Delta r_B/r^0_B(\log p_{O_2})$ dependences for $LaCr_{0.79}Co_{0.05}Al_{0.16}O_{3-\delta}$, the one calculated assuming Co^{2+} (LS) resembles $\Delta L/L_0(\log p_{O_2})$ better to the point that even the intersection of $\Delta r_B/r^0_B(\log p_{O_2})$ and $\Delta L/L_0(\log p_{O_2})$ for $La_{0.95}Ca_{0.05}Cr_{0.84}Al_{0.16}O_{3-\delta}$ and $LaCr_{0.79}Co_{0.05}Al_{0.16}O_{3-\delta}$ is at the same $\log p_{O_2}$ (see Fig. 3). Thus, it was assumed that the low-spin state is the most likely one for Co^{2+} in $LaCr_{0.79}Co_{0.05}Al_{0.16}O_{3-\delta}$.[120]

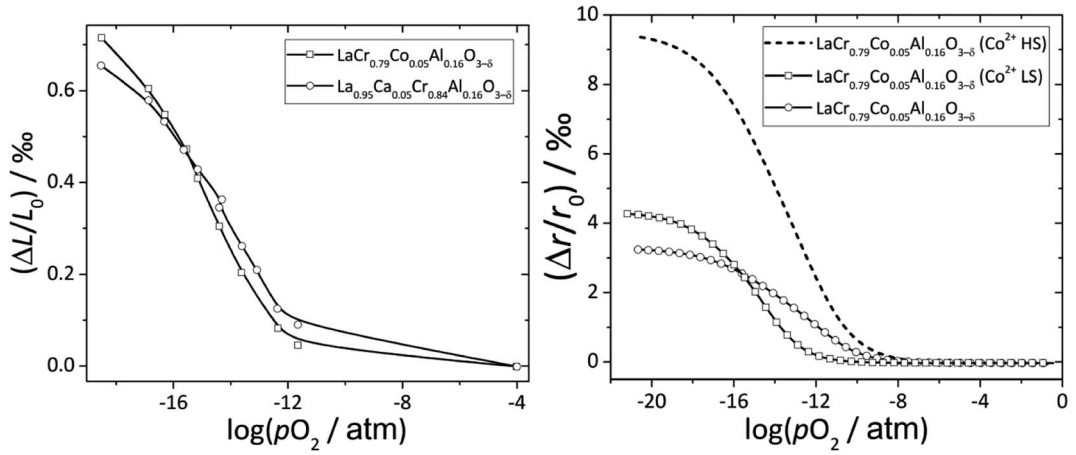

Fig. 3 $\Delta L/L_0 = f(\log p_{O_2})$ and $\Delta r_B/r^0_B = f(\log p_{O_2})$ dependences for $La_{0.95}Ca_{0.05}Cr_{0.84}Al_{0.16}O_{3-\delta}$ and $LaCr_{0.79}Co_{0.05}Al_{0.16}O_{3-\delta}$.[120]

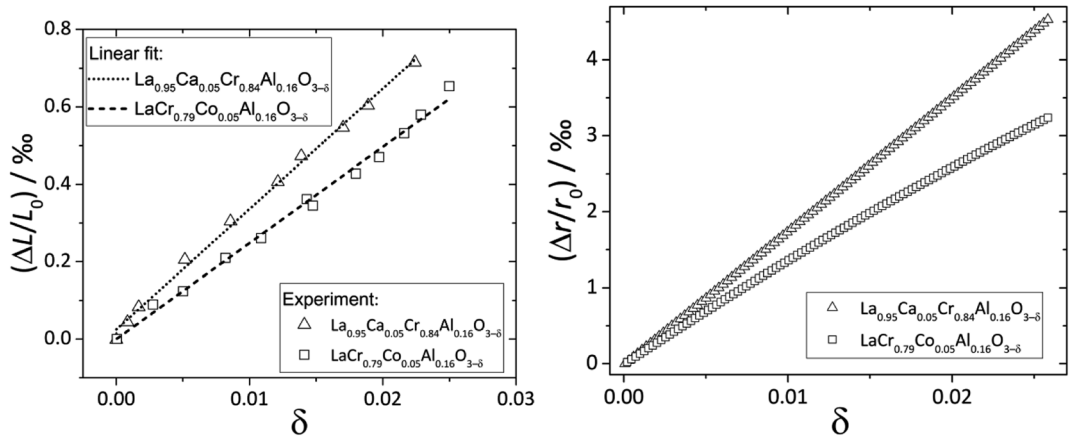

Fig. 4 $\Delta L/L_0 = f(\delta)$ and $\Delta r_B/r_B^0 = f(\delta)$ dependences for $La_{0.95}Ca_{0.05}Cr_{0.84}Al_{0.16}O_{3-\delta}$ and $LaCr_{0.79}Co_{0.05}Al_{0.16}O_{3-\delta}$.[120]

Later on, these promising, though only qualitative, observations[119,120] were developed into a quantitative chemical expansion model.[121,122] In its framework, the isotropic chemical strain of an oxide is approximated by that of a hypothetical crystal lattice formed by close-packed rigid spherical ions. It can be shown (see, for example, Tsvetkov *et al.*[123]) that the relative linear expansion of either the unit cell or the bulk of such a lattice is equal to the relative change in weighted mean ionic radius:

$$\varepsilon_{\text{chem}} = \frac{\Delta a}{a_0} = \frac{\Delta L}{L_0} = \frac{\sum_i (c_i r_i - c_{i0} r_i)}{\sum_i c_{i0} r_i}, \quad (32)$$

where c_i and r_i are the concentration and the crystal ionic radius[81] of an ith ion in an oxide, and the subscript 0 denotes the reference state where $a = a_0$ and $L = L_0$.

Among the initial explicitly made assumptions, or simplifications, in this model (eqn (32)) were the equality of oxygen ion and vacancy radii, $r_V = r_O$, and nonstoichiometry-independent coordination numbers of ions. One tricky implicit assumption which, however, is characteristic of all the models employing the ionic radii concept, deserves to be mentioned as well. It is a supposition that the values, or at least the ratios, of ionic radii derived from the room-temperature structural studies[81] are more or less valid at higher temperatures where *in situ* chemical expansion is usually observed and measured.

In contrast to the models of Miyoshi *et al.*[116] and Chen *et al.*[118] (see eqn (30) and (31)), all ions are taken into account in eqn (32) and not only those that are actually changing their oxidation state. In addition, both the numerator and denominator in eqn (32) are calculated in a similar fashion – *via* the ionic radii and not the experimentally determined values such as unit cell parameters. As a result, the model based on eqn (32) was first shown to describe well the chemical strain dependences for $LaCoO_{3-\delta}$,[121] $La_{1-x}M_xCrO_{3-\delta}$ (M = Ca, Sr) and oxygen-deficient $LaMnO_{3\pm\delta}$ (ref. 122) ($\varepsilon_{\text{chem}}$ of which the DFT calculations[124] severely overestimated).

As different spin states – high-spin (HS), low-spin (LS) or intermediate-spin (IS) – are characteristic of both Co^{2+} and Co^{3+} ions, and the ion size depends on the spin state,[81] it becomes an important factor influencing unit cell volume of Co-containing oxides. For example, Shafeie *et al.*[125] correlated the TEC change in a series of $La_2Co_{1+z}(Ti_{1-x}Mg_x)_{1-z}O_6$ perovskites with the change in the LS/HS Co^{3+} content. Gradual transition of Co^{3+} from LS through IS to HS with temperature is also known to occur in $LaCoO_{3-\delta}$ (ref. 126–128) and $La_{1-x}Sr_xCoO_{3-\delta}$ (ref. 129) oxides; such transition impacts TEC[130,131] and is one of the reasons for the larger, as compared with $LaFeO_{3-\delta}$ and $LaNiO_{3-\delta}$, TEC of $LaCoO_{3-\delta}$.[132]

In most cases, especially at high temperatures, spin states are unknown, so to define r_i in eqn (32) the spin states of Co ions should be somehow assumed. While for $LaCoO_{3-\delta}$ it was enough to suppose Co^{2+} (LS) and Co^{3+} (HS)[121] for the model to coincide with the experimental data, such an approach did not work for some other cobaltites. Thus, presuming some IS state, where Co^{n+} in different spin states coexisted within one oxide, $r_{Co^{n+}}$ in eqn (32) was replaced by

$$r_{Co^{n+}} = r_{Co^{n+}}(\text{HS})x + r_{Co^{n+}}(\text{LS})(1 - x), \quad (33)$$

where x is the fraction of high-spin Co^{n+}. The values of x can be found by fitting the modified eqn (32), $\varepsilon_{\text{chem}}(\delta,x)$, to the experimental $\varepsilon_{\text{chem}}(\delta)$ dependences. This was performed for $La_{1-x}Sr_xCoO_{3-\delta}$ (x = 0.2, 0.4, 0.7),[133] $(La_{1-x}Sr_x)_{0.99}Co_{0.9}Ni_{0.1}O_{3-\delta}$ (x = 0.3, 0.4),[133] $La_{0.7}Sr_{0.3}Co_{0.9}Fe_{0.1}O_{3-\delta}$,[17] $La_{0.8}Sr_{0.2}Co_{0.9}Ni_{0.1}O_{3-\delta}$,[18] and $La_{0.1}Sr_{0.9}Co_{0.8}Fe_{0.2}O_{3-\delta}$,[134] in all cases showing good coincidence between the fit results and the data, with an expected growth in the fitted values of x (*i.e.* the transition of Co^{n+} from LS to HS) with temperature. Similarly, to explain the temperature dependence of $\varepsilon_{\text{chem}}$ of $LaNi_{0.6}Fe_{0.4}O_{3-\delta}$ the spin state of Fe^{3+} was introduced as a variable into eqn (32) by analogy with eqn (33). In this oxide, only at high temperatures (900–1000 °C) were all Fe^{3+} ions found to be in the HS state.[135]

All Fe^{n+} ions were assumed to be in the HS state in the chemical expansion model of $Sr_{1-x}La_xFeO_{3-\delta}$ (x = 0, 0.6).[13] The model yielded similar chemical expansion coefficients for $La_{0.6}Sr_{0.4}FeO_{3-\delta}$ and $SrFeO_{3-\delta}$, $\beta \approx 0.0197$, and the calculated $\varepsilon_{\text{chem}}(\delta)$ dependences coincided with the experimental

data[136–140] for both oxides up to $\delta \approx 0.2$.[13] At the same time, Bae *et al.*[19,20] demonstrated recently that chemical expansion of $Sr_{1-x}La_xFeO_{3-\delta}$ ($x = 0.2, 0.5$) is less than that predicted by the model based on eqn (32) assuming high-spin-only Fe^{n+} ions, and can be described with this model only if some Fe^{n+} ions are in the LS state.

Among $Sr_{1-x}La_xFeO_{3-\delta}$, only for $SrFeO_{3-\delta}$ at $\delta > 0.3$ did the *in situ* high-temperature XRD and dilatometric data show much higher chemical strain, with $\beta \approx 0.0574$.[13] Such disagreement between the model and the measurement results was explained by oxygen vacancy ordering, typical of highly nonstoichiometric $SrFeO_{3-\delta}$ (ref. 13) as well as similar oxides such as $SrFe_{1-x}Ti_xO_{3-\delta}$,[141,142] impacting ε_{chem} values. This conclusion is qualitatively supported by the DFT simulation results, showing increasing oxygen vacancy polaron size with increasing δ in $Sr_{1-x}La_xFeO_{3-\delta}$ due to the vacancy ordering.[143]

Some tetragonal double perovskite oxides – both A-site-ordered such as $RBaCo_2O_{6-\delta}$ (R = rare-earth metal, sp. gr. *P*4/*mmm*) and B-site-ordered such as $Sr_2FeMoO_{6-\delta}$ (sp. gr. *I*4/*m*) – are known to exhibit anisotropic chemical strain with expansion and contraction along the *a* and *c* axes, respectively, resulting in very small volumetric expansion.[18,144,145] The chemical strain of these oxides, calculated with eqn (32), was shown to agree well with experimentally determined expansion along the *a* axis, $\varepsilon_{chem}(a)$.[123,145–147] Moreover, for $Sr_2FeMoO_{6-\delta}$, ε_{chem} of the cubic ($Fm\bar{3}m$) polymorph is almost equal to that calculated with the model (eqn (32)) as well as to $\varepsilon_{chem}(a)$ of its tetragonal polymorph.[123,146] This indicates a similar nature of expansion of tetragonal ordered and cubic disordered perovskites along the *a* axis.[146] Indeed, Cox-Galhotra *et al.*[148,149] based on the neutron diffraction results supposed that the primary reason for expansion of $RBaCo_2O_{6-\delta}$ (R = Nd, Pr) within the *ab* plane is the same as in the simple perovskite cobaltites, *i.e.* the increase of cobalt ion radii upon reduction.

In order to calculate the contraction of materials exhibiting anisotropic chemical strain, Tsvetkov *et al.*[123,146] introduced the so-called anisotropic ratio of chemical expansion, $\beta_{AR} = \varepsilon_{chem}(c)/\varepsilon_{chem}(a)$, where $\varepsilon_{chem}(c) = \Delta c/c_0$ and $\varepsilon_{chem}(a) = \Delta a/a_0$ are the normalized changes of the corresponding unit cell parameters. This coefficient β_{AR} is similar to Poisson's ratio, which characterizes the anisotropy of elastic properties of materials. The value of β_{AR} should depend largely on the crystal structure and also to some extent may vary with the oxide composition.[123] It was demonstrated that for tetragonal $Sr_2FeMoO_{6-\delta}$ and $GdBaCo_2O_{6-\delta}$ an assumption that $\beta_{AR} = -1$ allowed estimating $\varepsilon_{chem}(c)$ values in close agreement with the experimental ones.[123,145,146]

3.2.2. Hydration-induced lattice expansion. The next modification of the model based on eqn (32) was introduced so as to describe the hydration-induced expansion.[6] For the typical proton-conducting oxide hydration process, expressed as

$$O_O^{\times} + V_O^{\cdot\cdot} + H_2O \rightleftarrows 2OH_O^{\cdot}, \quad (34)$$

if Shannon radii[81] are used and $r_{V_O^{\cdot\cdot}} = r_{O_O^{\times}}$ hypothesized, direct application of eqn (32) yields negative chemical expansion, contradicting the experimental data.[6,65,67–69,150–161] Instead of making $r_{V_O^{\cdot\cdot}}$ within the model smaller than $r_{O_O^{\times}}$, the authors[6] adopted another approach – it was assumed that the formation of oxygen vacancy decreases the coordination numbers of neighboring cations. Basically, taking $r_{V_O^{\cdot\cdot}} < r_{O_O^{\times}}$ and assuming the CN of cations to be nonstoichiometry-dependent are two somewhat equivalent[72] ways of describing the same phenomenon – the crystal lattice relaxation around the oxygen vacancy. However, the latter way was regarded as beneficial because it contains no arbitrary parameters such as $r_{V_O^{\cdot\cdot}}$.

Within the framework of the modified model,[6] the cation coordination numbers in $ABO_{3-\delta}$ perovskites depend on oxygen nonstoichiometry as

$$\begin{cases} CN(A) = 12 - 4\delta \\ CN(B) = 6 - 2\delta \end{cases}. \quad (35)$$

If, as a first approximation, the cation radii decrease linearly with CN, then

$$\begin{cases} r_A = a + m\cdot CN = a + m(12 - 4\delta) \\ r_B = b + n\cdot CN = b + n(6 - 2\delta) \end{cases}, \quad (36)$$

where the coefficients *a*, *m*, *b* and *n* are obtained by fitting straight lines to the Shannon radii data.[6,81] Sereda *et al.*[6] demonstrated that the model based on eqn (32) and (36) describes satisfactorily the experimental data on chemical expansion caused by hydration for a number of proton-conducting perovskites, such as $BaCa_{(1+y)/3}Nb_{(2-y)/3}O_{3-\delta}\cdot xH_2O$ with $y = 0$–0.5 (BCN),[150–152] $BaZr_{1-y}Y_yO_{3-\delta}$ (BZY),[65,67–69,153,154] $BaZr_{1-y}Sc_yO_{3-\delta}$ (BZS),[154–158] $BaCe_{1-y}Y_yO_{3-\delta}$ (BCY)[67,159,160] and $La_{0.9}Sr_{0.1}ScO_{3-\delta}$.[161]

4. Atomistic insights

Modern computational methods such as molecular dynamics (MD) or density functional theory approach (DFT) allow the unit cell parameters that are more or less close to the experimental ones to be calculated, at least for CeO_2.[88,162] However, the magnitude of chemical strain has proven to be trickier to calculate accurately. But, most importantly, these methods allow semiquantitative insights into the mechanisms of this phenomenon, which is usually hard to acquire from the empirical knowledge only.

To simulate the chemical expansion with MD, some oxygen ions should be removed and the required number of cations (*e.g.*, Ce^{4+}) replaced by those with a lower oxidation state (*e.g.*, Ce^{3+}). While in real experiments these events, accompanied by the cation radius change, occur simultaneously and cannot be decoupled, it is possible to do so in MD simulations. By varying the short range repulsion terms of interatomic potential so as to make the Ce^{3+} size equal to that of Ce^{4+}, Marrocchelli *et al.*[12] calculated the effects of creating oxygen vacancies in such "equal-radii" supercells. The removal of the oxygen ion eliminates the electrostatic screening, causing the relaxation of cations away from the vacancy and more prominent shifting of anions towards it, resulting in net crystal lattice contraction. In other words, an effective oxygen vacancy size in ceria is less than

that of an oxygen ion. Similar results were obtained for substituted ceria and zirconia[12] as well as for some other fluorite oxides,[21] for which, in addition, a nonmonotonic dependence of r_V on the host cation radius, r_{host}, with a maximum at $r_{host} \cong r_{Ce^{4+}}$ was found.[21] Thus, MD results confirmed the chemical expansion mechanism that follows from the purely empirical Hong and Virkar's model.[72]

Ab initio DFT and equal-radii MD computations of Marrocchelli *et al.*[32] as well as DFT results of Jedvik *et al.*[70] paint the same picture of lattice relaxation around the oxygen vacancy as described above for another structural type of oxide – perovskites. Aidhy *et al.*[33] using the DFT approach demonstrated that charged oxygen vacancies cause lattice expansion for oxides with pyrochlore and rock-salt structures as well. However, in case of different structures even the qualitative results seem to be less unanimous than for the fluorites: for some perovskites ($SrTi_{1-x}Ga_xO_3$ and $La_{1-x}Sr_xGa_{0.8}Mg_{0.2}O_{3-\delta}$) DFT predicted $r_V \geq r_O$ – expansion upon anion vacancy formation.[32] In addition, by computing the defect-induced strain tensors, several studies found the oxygen vacancy in perovskites to be anisotropic, its shape being more correctly described by an ellipsoid.[70,163] Nonetheless, while the DFT method showed lattice contraction when $V_O^{\cdot\cdot}$ in $BaZrO_3$ is created,[64,70] atomistic simulations of $BaZrO_3$ and $SrTiO_3$ using shell-potential models revealed that, when averaged over all possible orientations of the defect within the crystal, the total volumetric effect from the $V_O^{\cdot\cdot}$ creation is negligible, *i.e.* $\beta_V \approx 0$.[70,163,164]

As for the quantitative results, different models and sets of interatomic potentials used in MD calculate different total chemical expansion coefficients. For example, for undoped ceria, the dipole polarizable ion model (DIPPIM)[12,165] yielded $\beta = 0.061$ at 1000 °C, very close to the $\beta = 0.061$ experimentally determined by Hull *et al.*[11] However, larger β values can be obtained from the experimental data of others: from 0.073 (δ = 0.12–0.18 in $CeO_{2-\delta}$)[92] to 0.092 (δ = 0.02–0.20)[82] and 0.101 (δ = 0.12–0.18),[92] depending on the nonstoichiometry range. These β values are much closer to those computed with the shell model: 0.075, 0.081 or 0.091 for different potential sets.[162] Different methods are also known to yield different results: for A- and B-site substituted $LaGaO_3$, MD visibly underestimates and DFT overestimates the experimentally measured relative expansion.[32] Marrocchelli *et al.*[32] believe it to be due to the small magnitude of the chemical strain value, calculated from the difference between the computed unit cell parameters, as the absolute crystal lattice parameters themselves exhibited much better agreement with the measurement results.[32] In this respect, an *ab initio* approach to calculating the chemical expansion coefficient *via* elastic dipole tensors, omitting the need for optimizing the lattice constants at each defect concentration, may be beneficial.[88,91]

Empirical models indicate that in order for chemical expansion to take place due to cation radius change, the charge carriers should be localized. The same conclusion can be reached using *ab initio* methods. As standard DFT functionals do not describe adequately the localized nature of f-electrons for Ce cations, the DFT + U approach is used to overcome this deficiency.[12,66,166] By varying the Hubbard term U, Marrocchelli *et al.*[166] demonstrated the strong dependence of β on the U value (or the degree of localization), while for the computed β to approach the experimental values, a very high degree of electron localization was required for both fluorites and perovskites ($CeO_{2-\delta}$ and $BaCeO_{3-\delta}$, respectively). Based on such conclusions, Perry *et al.*[111] explained the lower-than-expected chemical expansion of $La_{0.9}Sr_{0.1}Ga_{1-x}Ni_xO_{3-\delta}$ by increased charge delocalization. In a similar way, the magnitude of chemical expansion of barium oxyhydride, $BaTiO_{3-x}H_x$, was found to be more consistent with the delocalized electron model, which was also supported by the electrical conductivity and inelastic neutron scattering results.[167]

However, the influence of charge localization on chemical expansion of perovskites seems to be rather more complex. As was demonstrated recently by Marthinsen *et al.*,[168] depending on the electrostatic screening of oxygen vacancies, determined by the nature of B-site cations, chemical expansion in some perovskites may even be reduced by an increase in the Hubbard U term.

The importance of the defect charge was also highlighted by Aschauer and Spaldin,[169] whose DFT calculations allowed them to conclude that altering the defect charge state could be used purposefully to control the thin film geometry *via* chemical expansion by using the field effect, selectively adding or removing the charge carriers. This is an alternative to the more "obvious" chemo-mechanical actuation through defect concentration control by, for example, direct electrochemical oxygen pumping.[170]

Computational methods have been actively employed to elucidate the possible magnitude and nature of defect-induced stresses in thin films and at surfaces.[171–176] For example, the recent *ab initio* calculations showed that tensile or compressive strain stabilizes oxygen vacancies at complex oxide interfaces.[171] This was explained by the chemical expansion due to the defect formation relieving the stress,[172] and is closely related to the anisotropic – in directions parallel and normal to the interface – chemical strain observed with *in situ* TEM, scanning transmission electron microscopy (STEM), electron energy loss spectroscopy (EELS) and optical strain measurements in $Ce_{1-x}Pr_xO_{2-\delta}$ thin films on a YSZ substrate.[172,173] The anisotropic character of chemical expansion was also found in perovskite-based epitaxial thin films using XRD.[174] Both experimental and computational studies[175,176] showed that the nature of the substrate determines the presence of compressive or tensile in-plane strain in perovskite $La_{1-x}Sr_xCoO_{3-\delta}$ films, which impacts the oxygen vacancy concentration therein, influencing such properties as the oxygen evolution reaction (OER) activity,[175] oxygen surface exchange and diffusion.[176]

Due to the promise of higher efficiency of proton-conducting SOFCs, hydration-induced expansion became the focus of multiple studies, including the computational ones.[34,64,66,70] Similar to the oxide expansion upon oxygen loss that resulted from the crystal lattice shrinkage due to $V_O^{\cdot\cdot}$ creation and expansion due to the cation reduction, two factors cause the chemical strain upon hydration. In the water sorption process, eqn (34), the decrease in size $\varepsilon_{OH_O^{\cdot}}$ occurs when $OH_O^{\cdot}$ defects

replace $O_O^\times$, and the more pronounced increase, $-\varepsilon_{V_O^{\cdot\cdot}}$, follows from $OH_O^\cdot$ in place of $V_O^{\cdot\cdot}$:[34,64,70]

$$\varepsilon_{H_2O} = 2\varepsilon_{OH_O^\cdot} - \varepsilon_{V_O^{\cdot\cdot}} \quad (37)$$

As was pointed out in our previous work,[6] DFT-evaluated chemical expansion coefficient values for cerates and zirconates $(Ba,Sr)(Zr,Ce)_{1-y}(Y,In,Sc,Ga)_yO_{3-\delta}$ tend to vary significantly even within one study depending on calculation conditions – the size of the supercell,[70] proton defect trapping,[70] relative positions of dopant ions and defects inside the supercell[66,177] or temperature.[34] Note that the importance of the point defect placement for correct DFT + U simulation of mixed-valence materials had been pointed out earlier using reduced ceria as an example.[89] The temperature factor was investigated in detail by Løken *et al.*,[34] who found that not only do both individual contributions from $V_O^{\cdot\cdot}$ or $OH_O^\cdot$ to the chemical expansion and the total chemical strain depend on temperature, but also that the thermal expansion coefficient depends on the presence of defects. This computational evidence[34] in favor of cross-influences of thermal and chemical expansion is in line with the results of modulated temperature dilatometric measurements,[178] showing that a lower TEC is characteristic of a more defect-rich crystal lattice of $SrTiO_3$ or $SrZrO_3$. However, in another dilatometric study an opposite trend was found for the TEC of $SrFe_{0.35}Sn_{0.65}O_{3-\delta}$,[179] which indicates the strong dependence of TEC *vs.* defect concentration behavior on the oxide composition or crystal structure, or possibly both.

5. Some peculiarities and trends in the chemical expansion of oxides

5.1. Fluorites

Unfortunately, while the experimental $\varepsilon_{chem}(\delta)$ data are available in the literature for a number of (Pr, Tb, Y, Sm, Zr)-substituted ceria, their description and analysis are often much less thorough than those performed for $Ce_xGd_{1-x}O_{2-\delta}$ as described above. However, let us briefly summarize the main observations available in the current literature. The values of chemical expansion coefficients for some undoped and doped ceria are presented in the ESI (Table S1†).

Due to the higher reducibility of Pr^{4+} ions as compared with Ce^{4+}, chemical expansion of Pr-substituted CeO_2, $Ce_{1-x}Pr_xO_{2-\delta}$ and $Ce_{0.8}Pr_xTb_{0.2-x}O_{2-\delta}$ can be observed at high T even at ambient oxygen partial pressure (0.21 atm)[85,90,180] in contrast to pure ceria which requires a strongly reducing atmosphere.[82,84] Similar behavior is also typical of fluorite oxides substituted with redox active 3d-metal cations, *e.g.*, Mn-substituted YSZ.[181] For $Ce_{1-x}Pr_xO_{2-\delta}$ no vacancy clustering was detected, and their defect structure can be adequately described by an oxygen exchange reaction

$$2Pr_{Ce}^\times + O_O^\times \rightleftarrows V_O^{\cdot\cdot} + 2Pr_{Ce}^{'} + \frac{1}{2}O_2 \quad (38)$$

at $\delta < x/2$,[85] and eqn (18) at $\delta > x/2$ when all Pr^{4+} ions are already reduced to Pr^{3+}. Here, the $\varepsilon_{chem} = f(\delta)$ dependence is linear in both nonstoichiometry ranges, but has different slopes ($\beta_{Ce} > \beta_{Pr}$), which was qualitatively explained to be caused by the higher difference between the sizes of Ce ions than between Pr ones: $r(Ce^{3+}) - r(Ce^{4+}) = 0.173$; $r(Pr^{3+}) - r(Pr^{4+}) = 0.166$.[81]

Chemical expansion of $Ce_{1-x}R_xO_{2-\delta}$ (R = Y, Sm; $x = 0.1$–0.2) is almost temperature-independent at 700–1000 °C,[182] and, in addition, is nearly linear within the wide δ ranges. The chemical expansion coefficient, β, is almost independent of the concentration of Sm in $Ce_{1-x}Sm_xO_{2-\delta}$ and decreases with x for $Ce_{1-x}Y_xO_{2-\delta}$, while the β values of $Ce_{0.9}Y_{0.1}O_{2-\delta}$ and $Ce_{0.9}Sm_{0.1}O_{2-\delta}$ are almost equal.[182,183]

Substitution of Zr for Ce decreases the reduction enthalpy of $Ce_{1-x}Zr_xO_{2-\delta}$ leading to more facile oxygen exchange at higher p_{O_2}.[184] Because Zr^{4+} ions are smaller than Ce^{4+}, it is believed that they distort the crystal lattice so as to make the formation of smaller oxygen vacancies near Zr sites, which lowers the effective CN of Zr^{4+}, energetically favorable.[86] Unlike most substituted ceria, $Ce_{0.8}Zr_{0.2}O_{2-\delta}$ possesses β that increases with δ and exhibits nonlinear temperature dependence.[87] The chemical expansion coefficient of ceria with high Zr concentrations ($Ce_{0.5}Zr_{0.5}O_{2-\delta}$ and $Ce_{0.5}Zr_{0.4}Pr_{0.1}O_{2-\delta}$) is almost twice as low as that of $Ce_{0.9}Gd_{0.1}O_{2-\delta}$ and $Ce_{0.9}Pr_{0.1}O_{2-\delta}$ and does not depend on T or δ.

5.2. Cubic or 'quasicubic' (distorted) perovskites

The usage of substituted lanthanum chromites as SOFC interconnect materials led to their chemical expansion being investigated.[114,115] Armstrong *et al.*[114] suggested that both Coulomb repulsion between Cr cations and ≈13% growth in Cr ion size contributed to the chemical expansion upon reduction, the latter having a major effect. The average chromium oxidation state strongly influences the unit cell parameters of the chromites, which is why introducing an acceptor dopant (Sr or Ca) into $La_{1-x}(Sr,Ca)_xCrO_{3-\delta}$ leads to a linear unit cell volume decrease.[114,115] The increase in x in $La_{1-x}M_xCrO_{3-\delta}$ (M = Sr, Ca) increases the chemical expansion of these oxides because of the growth in the fraction of "reducible" Cr^{4+} ions (see ESI Table S2†).[114,115,185,186] Likewise, some B-site dopants affect the chemical strain of $La_{1-x}M_xCrO_{3-\delta}$ (M = Sr, Ca) in accordance with their oxidation numbers: isovalent dopants (*e.g.* Al^{3+}) hardly change it while those with higher valences (*e.g.* Ti^{4+}) tend to decrease it.[114,115] Cerium ions, being substituted for La in $La_{1-x}Ca_xCrO_{3-\delta}$, cause ε_{chem} to be temperature-dependent because of the shifting $Ce^{3+} + Cr^{4+} \rightleftarrows Ce^{4+} + Cr^{3+}$ equilibrium.[185] Somehow counterintuitively, despite having to increase the Cr^{4+} fraction, introducing Mg into $LaCr_{1-x}Mg_xO_{3-\delta}$ decreases $\varepsilon_{chem} = \Delta a/a_0$, which is thought to be due to the large size of Mg^{2+} expanding the unit cell, *i.e.* increasing the value of a_0.[115]

Substituted lanthanum chromites exhibit oxygen exchange only at sufficiently low p_{O_2} ($p_{O_2} < 10^{-8}$ atm at 1000 °C).[114,119,120] In contrast, $La_{1-x}Sr_xMnO_{3\pm\delta}$ where oxygen excess ($3 \pm \delta > 3$) in the crystal lattice can be realized tend to release or take up O_2 at higher p_{O_2} as well, having plateaus on $\delta(\log(p_{O_2}))$ dependences between oxygen-excess and oxygen-deficient regions.[117,122,187–189] These two regions differ significantly in the defect chemistry: the oxygen adsorbed by the oxide fills the oxygen vacancies at $3 \pm \delta < 3$,

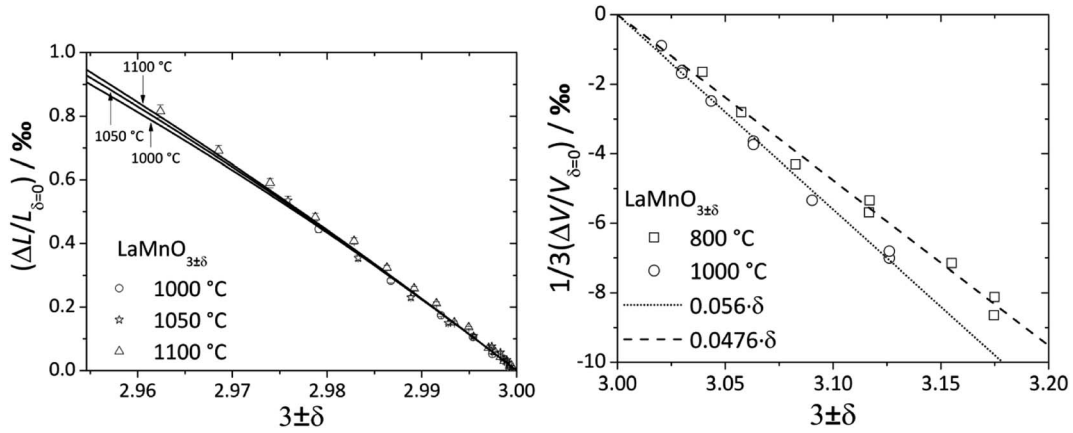

Fig. 5 Chemical expansion of $LaMnO_{3\pm\delta}$ with $3 \pm \delta < 3$ (ref. 122) and $3 \pm \delta > 3$:[189] solid lines – model calculations,[122] dashed lines – linear fit.

$$V_O^{\cdot\cdot} + 2Mn_{Mn}^{\times} + \frac{1}{2}O_2 \rightleftarrows 2Mn_{Mn}^{\cdot} + O_O^{\times}, \quad (39)$$

and leads to the Schottky-type disordering with cation vacancy formation at $3 \pm \delta > 3$,[122]

$$6Mn_{Mn}^{\times} + \frac{3}{2}O_2 \rightleftarrows V_{La}^{'''} + V_{Mn}^{'''} + 3O_O^{\times} + 6Mn_{Mn}^{\cdot}, \quad (40)$$

which was confirmed by neutron diffraction, SEM and TEM.[188,190] As a consequence, chemical expansion of oxygen-deficient $LaMnO_{3\pm\delta}$, which is mostly due to reduction of manganese ions (eqn (39)), was more or less successfully described in the frameworks of the appropriate models based on the cation radius change (eqn (30) or (32)).[116,122]

For $LaMnO_{3\pm\delta}$ with $3 \pm \delta > 3$, despite prolonged relaxation times and noticeable creep, dilatometric experiments showed visible sample expansion,[188] but XRD showed unit cell volume contraction[189] with increasing p_{O_2}. As shown in Fig. 5, the value of β for the oxygen-excess $LaMnO_{3\pm\delta}$ (0.0476–0.056 (ref. 189)) is almost twice as high as that for the oxygen-deficient one (0.024 (ref. 116)). Similar observations were made for strontium-substituted manganites $La_{1-x}Sr_xMnO_{3\pm\delta}$.[109] The seeming contradiction between dilatometric and XRD results[188,189] could be explained by the expansion of the crystal lattice due to the Schottky reaction (eqn (40)) being stronger than its contraction due to the Mn^{3+} oxidation. In other words, the expansion of the oxide bulk due to eqn (40) as measured by dilatometry should be greater than the average unit cell parameter increase detected by XRD.

The discrepancies between the defect structure models used for $La_{1-x}Sr_xM_{1-y}B_yO_{3-\delta}$ (M = Co, Ni, Fe; B = Co, Ni, Fe; M ≠ B) are primarily related to the issue of charge localization. In some models, such as the "itinerant electron" or Lankhorst model,[191–194] it is supposed that most electrons are located within the conduction band. While these models typically describe experimental $\delta = f(p_{O2})$ dependences as well as those with localized charge carriers,[195–197] for chemical expansion to occur, cation reduction ought to take place,[10,32,118] so most, if not all, electrons and holes should be localized. Thus, the models where the oxygen release from the crystal lattice of $La_{1-x}Sr_xM_{1-y}B_yO_{3-\delta}$ is represented by the following process

$$2M_M^{\cdot} + O_O^{\times} \rightleftarrows V_O^{\cdot\cdot} + 2M_M^{\times} + \frac{1}{2}O_2, \quad (41)$$

and charge disproportionation or exchange can be written as

$$2M_M^{\times} \rightleftarrows M_M^{\cdot} + M_M^{'}, \quad (42)$$

$$M_M^{\times} + B_M^{\times} \rightleftarrows M_M^{\cdot} + B_M^{'}, \quad (43)$$

where $M_M^{\cdot}$ and $M_M^{'}$ are localized holes and electrons, respectively, received more attention in papers dealing with chemical expansion.[94,108,121,195–201] If two different cations that are able to change their oxidation state, *e.g.* Cr, Mn, Fe, Co, or Ni, occupy the B-sublattice of $La_{1-x}Sr_xM_{1-y}B_yO_{3-\delta}$, and the fraction of one of them is significantly greater, eqn (42) can be used in the defect structure model along with either fixing the oxidation state of the other one[200] or assuming M and B ions to be indistinguishable within the model's framework.[134,199] In case the M and B concentrations are close, the model usually incorporates eqn (43) taking into account the respective electronegativities of B and M, *e.g.* M = Co if B = Ni or M = Fe if B = Co, because $\chi_{Fe} = 1.64$, $\chi_{Co} = 1.70$ and $\chi_{Ni} = 1.75$.[195,202]

Many of $La_{1-x}Sr_xM_{1-y}B_yO_{3-\delta}$ and $Ba_{1-x}Sr_xCo_{1-y}Fe_yO_{3-\delta}$ oxides release oxygen upon heating even at high oxygen partial pressures, *e.g.* in air. Therefore, characteristic chemical-expansion-related deviations from near linear trends are observed in high-temperature regions of dilatometric curves $\varepsilon = f(T)$ of these oxides.[118,203–208] An assumption that both thermal and chemical expansion coefficients are temperature-independent, $\varepsilon(T,\delta) = \varepsilon_{chem}(\delta) + \varepsilon_{therm}(T) = \alpha\Delta T + \beta\Delta\delta$, allows β to be estimated from total expansion, *i.e.* the dilatometric $\varepsilon(T,\delta)$ curves. The value of α can be determined from the low-temperature $\varepsilon(T,\delta)$ region where no oxygen exchange occurs, and $\delta(T)$ can be measured with thermogravimetric analysis (TGA).[23,118,203,209]

The nonlinearity of $\varepsilon_{chem}(\delta)$ for $(La_{1-x}Sr_x)_{0.99}Co_{1-y}Ni_yO_{3-\delta}$ and $La_{1-x}Sr_xCoO_{3-\delta}$, which was described[118,203] by the equation $\beta = \beta_1 + \beta_2\delta$, is quite small and can be neglected within a relatively narrow δ range, *e.g.* when ε_{chem} at one temperature is considered. In contrast, the temperature dependences of β for these oxides, shown in Fig. 6, are more pronounced. A gradual increase in the fraction of HS Co^{3+} with temperature was

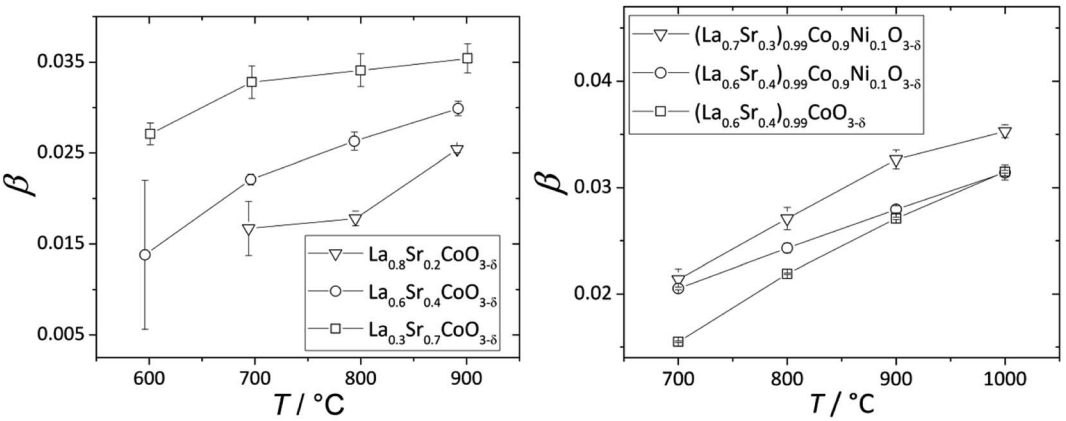

Fig. 6 Temperature dependences of β for $La_{1-x}Sr_xCoO_{3-\delta}$ (ref. 118) and $(La_{1-x}Sr_x)_{0.99}Co_{1-y}Ni_yO_{3-\delta}$.[203]

assumed to be the likely reason behind such dependences.[17,18,133,134] An increase in β with T was also observed for $La_{0.5}Sr_{0.5}Fe_{0.5}Co_{0.5}O_{3-\delta}$,[206] $La_{0.1}Sr_{0.9}Fe_{0.2}Co_{0.8}O_{3-\delta}$ (ref. 134) and some ferrites, such as $La_{0.3}Sr_{0.7}Fe_{0.6}Ga_{0.4}O_{3-\delta}$,[204] $La_{0.3}Sr_{0.7}FeO_{3-\delta}$,[204] $SrTi_{0.65}Fe_{0.35}O_{3-\delta}$,[112] and $La_{0.2}Sr_{0.8}Fe_{0.55}Ti_{0.45}O_{3-\delta}$.[201] Some evidence exists for the possibility of Fe^{3+}(LS) → Fe^{3+}(HS) transition in perovskites at elevated temperatures,[210] so this,[112,135] along with some degree of charge delocalization, changes in B-site coordination and subtle crystal symmetry changes[112] might also be responsible for the temperature-dependent chemical expansion of iron-containing perovskites. Interestingly, inverse trends – lower β at higher T – were reported for $Ba_{0.5}Sr_{0.5}Co_{0.8}Fe_{0.2}O_{3-\delta}$ (ref. 205, 207, 211 and 212) and $SrCo_{0.8}Fe_{0.2}O_{3-\delta}$,[212] and the reason behind this is yet unclear.

Some other trends in β of $La_{1-x}Sr_xCo_{1-y}Fe_yO_{3-\delta}$ and $La_{1-x}Sr_xCo_{1-y}Ni_yO_{3-\delta}$ can be tentatively established (see also Table S3 in the ESI†). For instance, substituting Sr for La increases β of $La_{1-x}Sr_xCoO_{3-\delta}$,[118,121] $La_{1-x}Sr_xFe_{0.2}Co_{0.8}O_{3-\delta}$ (ref. 134, 198 and 199) and $(La_{1-x}Sr_x)_{0.99}Co_{1-y}Ni_yO_{3-\delta}$ (ref. 203) (see Fig. 6). The slight A-sublattice substoichiometry and up to 10% substitution of Ni for Co in the B sublattice hardly change β.[118,203] At the same time, for $La_{0.6}Sr_{0.4}Fe_{1-x}Co_xO_{3-\delta}$ oxides no obvious relationship between the B-sublattice composition and chemical expansion coefficient can be observed.[198,213,214] This may be because the temperature dependence of β, which may be strong and also composition-dependent for these oxides, was not taken into account in the respective studies.[198,213,214]

For some $La_{1-x}Sr_xFeO_{3-\delta}$, existing chemical expansion data are contradictory: for example, β reported for $La_{0.5}Sr_{0.5}FeO_{3-\delta}$ (ref. 20 and 215) and $La_{0.6}Sr_{0.4}FeO_{3-\delta}$ (ref. 198 and 216) in separate papers differs almost by a factor of two. Nonetheless, it can be said that, similarly to $La_{1-x}Sr_xCoO_{3-\delta}$,[118] the chemical expansion coefficient of $La_{1-x}Sr_xFeO_{3-\delta}$ tends to increase with Sr content.[13,19,20,198,204,215,216] In fact, alkaline earth metal ferrites such as $SrFeO_{3-\delta}$ (ref. 13) (and also $Ba_{0.95}La_{0.05}FeO_{3-\delta}$ (ref. 217)) demonstrate chemical expansion that is among the highest for all perovskite-like oxides (see ESI Tables S2 and S3†). As was noted above, such high ε_{chem} may be caused by the oxygen vacancy ordering in these highly nonstoichiometric oxides.[13,19,20,108,143] In addition, and in support of the assertion that it is high nonstoichiometry that causes elevated chemical expansion, visibly nonlinear ε_{chem} with β increasing at higher δ was observed on both isotropic and anisotropic $\varepsilon_{chem}(\delta)$ dependences for $La_{1-x}Sr_xFeO_{3-\delta}$ ($x = 0.2$–0.5).[19,20,108]

B-site substitution with ions that do not change their oxidation state, such as Al or Ga, causes different chemical expansion changes in different ferrite perovskites. For example, β of $La_{0.8}Sr_{0.2}Fe_{0.7}Ga_{0.3}O_{3-\delta}$ is greater than that of $La_{0.8}Sr_{0.2}FeO_{3-\delta}$,[19,218] while replacing Fe in $SrFeO_{3-\delta}$ with Al (or Ti) leads to the opposite effect of decreasing β;[13,112,219] in both cases the high-temperature crystal lattice symmetry after the substitution remained practically unchanged.[13,112,215,218,219] Though they have lower chemical expansion than $SrFeO_{3-\delta}$, $SrFe_{1-x}Ti_xO_{3-\delta}$ oxides, which have been extensively studied lately as promising cobalt-free mixed ion–electron conductors (MIECs),[220] still possess fairly high β, above that of most $La_{1-x}Sr_xCo_{1-y}Fe_yO_{3-\delta}$.[112,201] As compared with $SrFe_{0.35}Ti_{0.65}O_{3-\delta}$, $SrFe_{0.35}Sn_{0.65}O_{3-\delta}$ is characterized by lower chemical expansion coefficient values, and the opposite trends in both TEC and β: the TEC of $SrFe_{0.35}Sn_{0.65}O_{3-\delta}$ decreases with δ, and β decreases with temperature.[112,179] This is believed to be due to the asymmetric (close to tetragonal) crystal structure of $SrFe_{0.35}Sn_{0.65}O_{3-\delta}$ as compared with the almost cubic $SrFe_{0.35}Ti_{0.65}O_{3-\delta}$.[179]

Based on the TG and dilatometric studies into $Nd_{1-x}Sr_xFe_{0.7}Co_{0.3}O_{3-\delta}$ (ref. 221) and $Nd_{1-x}Sr_xFeO_{3-\delta}$,[222] similarly to $La_{0.6}Sr_{0.4}Fe_{1-x}Co_xO_{3-\delta}$,[114,130,131] no apparent influence of Co substitution on β can be stated. It can also be concluded that, on average, β of $Nd_{1-x}Sr_xFe_{0.7}Co_{0.3}O_{3-\delta}$ (ref. 221) and $Nd_{1-x}Sr_xFeO_{3-\delta}$ (ref. 222) is greater than that of their La-containing analogs. However, the data on chemical expansion of $R_{1-x}Sr_xCo_{1-y}Fe_yO_{3-\delta}$ where R is a rare-earth metal other than La are rather scarce, so the influence of the nature of the A-site rare earth ion on ε_{chem} remains largely speculative.

5.3. Double perovskites

In contrast to simple perovskites, for which the deviations from cubic symmetry are caused by slight twists and distortions of the oxygen octahedra,[223,224] the tetragonal (and orthorhombic) symmetry of double perovskites is due to cation ordering.[225] For

that reason, strong anisotropy of chemical expansion is typical of many double perovskites. Among the A-site ordered layered double perovskites, chemical expansion studies were primarily focused on $RBaM_2O_{6-\delta}$ (M = Co, Fe).[31,123,144,148,149,226–238] Although the literature data are mostly rather scattered (see Table S4 in the ESI†), some common trends can nevertheless be established.

As mentioned in Section 3.2.1, tetragonal $RBaM_2O_{6-\delta}$ (M = Co, Fe) oxides tend to expand along the *a* axis (or in the *ab* plane) with the decrease in δ, which is most probably because of the increase in 3d metal cation radii upon their reduction.[148,149] Along the *c* axis, both the chemical strain $\varepsilon_{chem}(c)$ and chemical expansion coefficient β_c are negative. It is known that oxygen vacancies in these double perovskites form predominantly at O3 sites, *i.e.* within the rare-earth layers.[239–242] Hence, simultaneous contraction of the unit cell along the *c* axis, in the direction normal to the R^{3+} and Ba^{2+} cation layers, can be qualitatively explained by the shifting of nearby ions (Co1 or Fe1 and O2) in the direction of RO planes.[148,149] This may also be responsible for the composition-dependent β_c observed for $RBaFe_2O_{6-\delta}$ (R = Pr, Nd, Sm, Eu, Gd), shown in Fig. 7. A decrease in the R^{3+} effective radius should lower the electrostatic repulsion, allowing the nearby ions to shift farther towards the RO layers when they are filled with oxygen vacancies, thus making β_c higher for $RBaFe_2O_{6-\delta}$ with smaller R.[226–232] At the same time, β_a coefficients for all $RBaFe_2O_{6-\delta}$ (R = Pr, Nd, Sm, Eu, Gd) are much closer to each other than β_c, only slightly growing with the R^{3+} radius (see ESI Table S4†).

On average, chemical expansion of the unit cell parameter *a* for both layered double cobaltites[31,123,144,148,149,233–235] and ferrites[226–232] $RBaM_2O_{6-\delta}$ (M = Co, Fe) is quite similar, which is somehow expected due to the equal difference between the "reducible" ion radii (at least in their HS states): $r(Co^{3+}) - r(Co^{2+}) = r(Fe^{3+}) - r(Fe^{2+})$.[81] One clear exception is $LaBaCo_2O_{6-\delta}$,[236–238] for which both expansion of *a* and contraction of *c* are higher than for the other $RBaCo_2O_{6-\delta}$ (R = Pr, Nd, Gd).[31,123,144,148,149,233–235] Bernuy-Lopez *et al.*[236] even claimed the expansion of $LaBaCo_2O_{6-\delta}$ along the *c* axis, but their data are inconsistent across the plots presented in the article, and neither their nonstoichiometry values nor crystallographic data are supported by other studies.[243–245]

The values of β_c, however, are several times greater (by absolute value) for $RBaFe_2O_{6-\delta}$ (ref. 226–232) than for $RBaCo_2O_{6-\delta}$ (see Table S4 in the ESI†).[31,123,144,148,149,233–238] However, in contrast to $RBaCo_2O_{6-\delta}$, where the expansion data were mostly collected at high temperatures,[31,123,144,148,149,233–238] the chemical expansion of $RBaFe_2O_{6-\delta}$ (ref. 226–232) (see Fig. 7) refers to the quenched samples and was measured near room temperature. Under these conditions strongly anisotropic magnetic ordering is known to arise in $RBaFe_2O_{6-\delta}$: for example, iron in its mixed-valent state in $TbBaFe_2O_5$ exhibits antiferromagnetic super-exchange coupling through oxygen ion and ferromagnetic coupling – through oxygen vacancies across the Tb layer, while the bulk of the material remains antiferromagnetic.[246] In addition, mixed-valent iron is known to have a smaller volume than the corresponding average of the HS Fe^{2+} and Fe^{3+}.[232,247] This and the nonstoichiometry-dependent magnetic interactions along the *c* axis of these layered ferrites[246] may be responsible for the large contraction of their unit cells in that direction.

As seen in Fig. 8, where the measurement results at similar temperatures are presented for $RBaCo_2O_{6-\delta}$ (R = Pr, Nd, Gd), $\beta_a \approx -\beta_c$ for these double perovskite cobaltites, and their chemical expansion is close, taking into account the scatter in the data.[123,148,149] However, when all available experimental data for each of these oxides are considered,[31,123,144,148,149,233–235] it is immediately seen (Fig. S1–S3 in the ESI†) that the $\varepsilon_{chem}(\delta)$ values do not often coincide well except for $GdBaCo_2O_{6-\delta}$, for which the results of Mogni *et al.*,[233] Tsvetkov *et al.*[123] and Chatterjee *et al.*[31] agree with each other in the overlapping δ ranges. The smaller β_c of $GdBaCo_2O_{6-\delta}$ at $\delta < 0.5$ (ref. 31) (see ESI Fig. S1†) is likely, at least in part, because in this range the oxygen loss leads predominantly to $Co^{4+} \rightarrow Co^{3+}$ reduction causing a smaller ionic radius change as compared to $Co^{3+} \rightarrow$

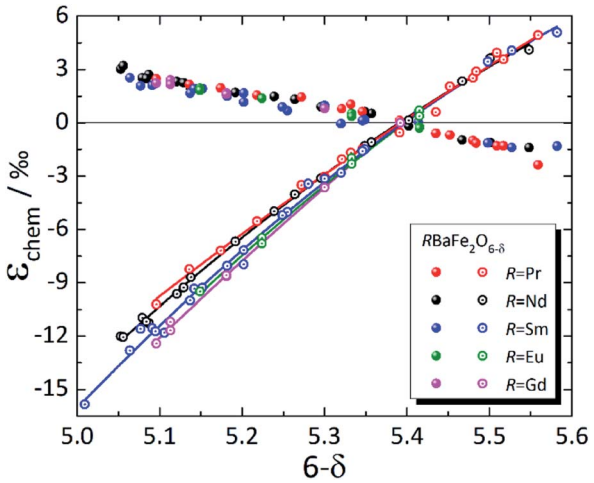

Fig. 7 Chemical strain of $RBaFe_2O_{6-\delta}$ (R = Pr,[226] Nd,[227,228] Sm,[228–230] Eu,[231] Gd[232]), measured at *T* up to 47 °C. Filled symbols – $\varepsilon_{chem}(a)$; empty symbols – $\varepsilon_{chem}(c)$; lines are given to guide the eye only.

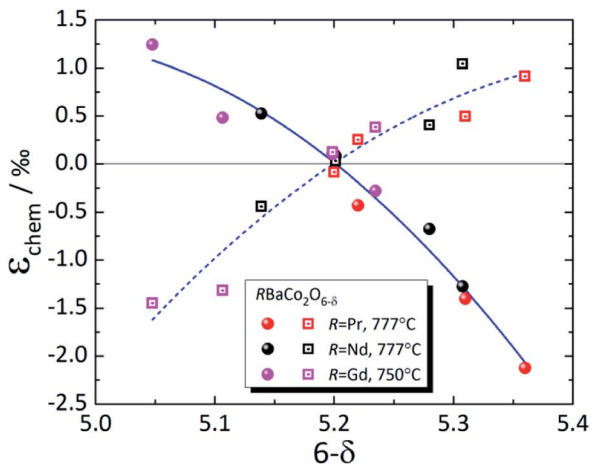

Fig. 8 Chemical strain of $RBaCo_2O_{6-\delta}$ (R = Pr,[149] Nd,[148] Gd[123]). Filled symbols – $\varepsilon_{chem}(a)$; empty symbols – $\varepsilon_{chem}(c)$; lines are given to guide the eye only.

Co^{2+} at $\delta > 0.5$.[81] A similar change in the slope of $\varepsilon_{chem}(\delta)$ at $\delta \approx 0.5$ is seen in Fig. 7 as slight nonlinearities on the respective dependences for $RBaFe_2O_{6-\delta}$ (R = Pr, Nd, Sm, Eu, Gd).[226–232]

The strong discrepancies between $\varepsilon_{chem}(\delta)$ of $RBaCo_2O_{6-\delta}$ (R = Pr, Nd) reported by Cox-Galhotra *et al.*[148] and Szpunar *et al.*[234] are probably due to several reasons. First of all, in the work of Szpunar *et al.*[234] $RBaCo_2O_{6-\delta}$ (R = Pr, Nd) are orthorhombic in wide δ ranges ($\Delta\delta \approx 0.5$), which is in contrast to previous studies where orthorhombic symmetry, which is due to oxygen vacancy ordering, was found to be present only at δ close to 0.5.[239] Then, the $\varepsilon_{chem}(\delta)$ therein[234] was determined not from the isothermal experiment results, as in ref. 148 and 149, but from the temperature dependences of unit cell parameters by subtracting the low-temperature linear trend from the total ε values assuming temperature-independent TEC. In this respect, the volumetric chemical expansion of $NdBaCo_2O_{6-\delta}$ determined in a similar manner by Cherepanov *et al.*[248] from the dilatometric experiments coincides with that measured by Szpunar *et al.*,[234] but is visibly greater than that found by Cox-Galhotra *et al.*[148] (see Fig. S4 in the ESI†). This may be accounted for by supposing that the TEC of $NdBaCo_2O_{6-\delta}$ actually increases with temperature, neglecting which would cause the calculated chemical expansion to be overestimated by the value of this increase.[234,248]

As opposed to $RBaFe_2O_{6-\delta}$,[226–232] both β_a and β_c of $RBaFeCuO_{6-\delta}$ (R = Lu, Yb, Y, Eu, Sm, Nd, Pr) oxides are negligible (see also ESI Fig. S5†).[249–251] The oxidation state of Cu^{2+} forces iron in $RBaFeCuO_{6-\delta}$ to assume higher oxidation states at $\delta > 0.5$ than in $RBaFe_2O_{6-\delta}$. Hence, the oxygen release from $RBaFeCuO_{6-\delta}$ is accompanied by $Fe^{4+} \rightarrow Fe^{3+}$ reduction, causing much lower ionic radius changes and much lower expansion.[249,250] The absence of contraction of the unit cell parameter c with δ in $RBaFeCuO_{6-\delta}$ (ref. 251) might be related to the crystal structure of these oxides, where corner-sharing strongly elongated CoO_5 and already squashed FeO_5 pyramids[252] have little opportunity to shift towards oxygen-depleted rare-earth layers.

Kudyakova *et al.*[147] reported that substituting Mn for Fe in $PrBaFe_2O_{6-\delta}$ results in a pronounced decrease in β_c measured at room temperature, down to almost zero for $PrBaMn_2O_{6-\delta}$, while β_a of both $PrBaFeMnO_{6-\delta}$ and $PrBaMn_2O_{6-\delta}$ are almost equal and more than two times greater than that of $PrBaFe_2O_{6-\delta}$ (see ESI Fig. S5 and Table S4†). Tomkiewicz *et al.*,[253] on the other hand, found with *in situ* neutron diffraction that both a and c parameters of $PrBaMn_2O_{6-\delta}$ increase upon reduction; unfortunately, there is not yet enough data to speculate whether such discrepancy between two studies[147,253] is caused by different temperature and nonstoichiometry ranges (see Table S4 in the ESI†) or something else.

5.4. Oxides with a Ruddlesden–Popper structure

The crystal structure of layered Ruddlesden–Popper oxides $A_{n+1}B_nO_{3n+1}$ may be represented as alteration of n successive perovskite ABO_3 layers with one rock-salt AO layer. The most well-studied compounds in this family of oxides are those with $n = 1$ possessing a K_2NiF_4 structure (space group $I4/mmm$). These oxides can accumulate interstitial oxygen in the rock-salt layers[254] and oxygen vacancies – in the perovskite ones,[255] attaining oxygen excess $(4 + \delta)$ or deficiency $(4 - \delta)$, respectively.

The oxygen-excess $La_{2-x}Sr_xNiO_{4+\delta}$,[256–258] $La_2(Ni_{0.9}M_{0.1})O_{4+\delta}$ (M = Fe, Co, Cu)[254,258] and $Nd_{2-x}Sr_xNiO_{4+\delta}$ (ref. 259) expand in the *ab* plane upon oxygen loss because of the nickel cation reduction. This is accompanied by a significant decrease of the unit cell parameter c, which may be related to the weakening of electrostatic repulsion between ions as interstitial oxygen leaves the crystal lattice.[256] As a result, as for many double perovskites,[31,123,144,148,149,226–235] the volumetric chemical expansion of Ruddlesden–Popper oxides is almost zero or even negative:[10,254,256,257,259] for example, for $La_2NiO_{4+\delta}$, $\beta_a = -0.028$, $\beta_c = 0.076$, and $\beta = 0.002$.[10,256] Substitution of small amounts of Fe, Co or Cu for Ni in $La_2NiO_{4+\delta}$ increases, by an absolute value, its chemical strain along the a axis, while β_c remains almost unchanged.[254]

Similar to that of substituted $La_2NiO_{4+\delta}$ (ref. 254 and 256–258) chemical strain behavior – expansion of a and contraction of c unit cell parameters upon reduction – was also found in $Sr_3Fe_2O_{7-\delta}$ and $Sr_3Fe_{1.9}Mo_{0.1}O_{7-\delta}$;[255,260] the molybdenum-doped sample was characterized by lower thermal and chemical expansion.[255]

In contrast to $Sr_3Fe_2O_{7-\delta}$, both a and c parameters of $Sr_3FeCoO_{7-\delta}$ increased with δ ($\beta_c > \beta_a > 0$), which was believed[260] to be due to the charge delocalization in $Sr_3FeCoO_{7-\delta}$ that decreased the electrostatic interactions, potentially responsible for the contraction along the c axis. Oxygen-deficient $(R_{2-x}Sr_x)_{0.98}(Fe_{0.8}Co_{0.2})_{1-y}Mg_yO_{4-\delta}$ (R = La, Pr) also exhibit expansion upon reduction along the a and c axes;[261] in this case, the fact that $\beta_c > \beta_a$ was explained by the nearby rock-salt layers effectively limiting the ability of the perovskite layers to expand within the *ab* plane.[261] The volumetric chemical expansion of these $(R_{2-x}Sr_x)_{0.98}(Fe_{0.8}Co_{0.2})_{1-y}Mg_yO_{4-\delta}$ is much lower than that of the simple perovskites with similar composition, such as $La_{0.6}Sr_{0.4}Fe_{0.8}Co_{0.2}O_{3-\delta}$.[262]

6. Some consequences of chemical expansion and its possible practical applications

The most straightforward consequence of excessive chemical strain, similar to unwanted thermal expansion, is the mechanical failure of ceramic materials and devices. Various examples of this, some of which are quite graphic, can be readily found in the literature.[9,24,47,49,263–266] For example, Fig. 9a and b show the microcracks occurring in lithium-ion battery cathodes,[25] and Fig. 9c demonstrates the pinhole and crack formation in the ceria-based SOFC electrolyte, caused by the reduction-induced chemical expansion of ceria.[24] In the latter case, dynamic load conditions, resulting in varying oxygen partial pressure gradients, were found to exacerbate the SOFC degradation.[24]

The fact that chemical strain can lead to mechanical failure is particularly well known in the field of solid-state battery development, since many widely employed Li-ion conducting materials experience large chemical expansion—up to several

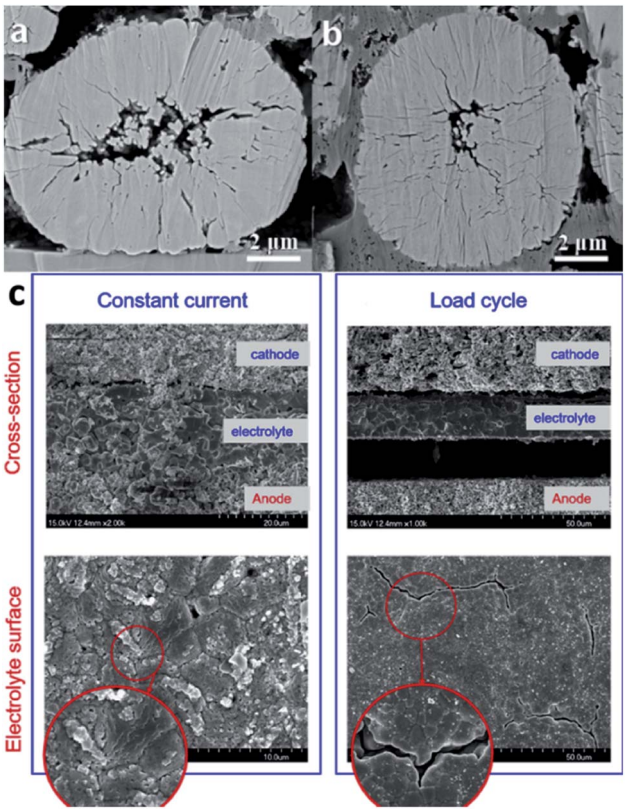

Fig. 9 Failure of electrochemical devices due to chemical expansion. (a and b) Cross-sectional SEM images of the $Li_{1-\delta}[Ni_{0.6}Co_{0.2}Mn_{0.2}]O_2$ (a) and $Li_{1-\delta}[Ni_{0.8}Co_{0.1}Mn_{0.1}]O_2$ (b) cathodes in the fully charged state; reprinted with permission from H.-H. Ryu, K.-J. Park, C. S. Yoon and Y.-K. Sun, *Chem. Mater.*, 2018, **30**, 1155–1163. © 2018 American Chemical Society.[25] (c) Post-mortem analysis of the SOFC (NiO–$Nd_{0.1}Ce_{0.9}O_{2-\delta}$ composite anode, $Nd_{0.1}Ce_{0.9}O_{2-\delta}$ electrolyte, $NdBa_{0.5}Sr_{0.5}Co_{1.5}Fe_{0.5}O_{5+\delta}$ cathode) under constant current (0.2 A cm^{-2}) and load cycle (0.2–0.12 A cm^{-2}) conditions at 650 °C; reprinted from Y.-D. Kim, J. Yang, J.-I. Lee, M. Saqib, J.-S. Shin, K. Park, M. Jo, S.-J. Song and J.-Y. Park, Degradation studies of ceria-based solid oxide fuel cells at intermediate temperature under various load conditions, *J. Power Sources*, **452**, 227758, © 2020, with permission from Elsevier.[24]

percents—upon lithiation/delithiation.[47,49,60,265,267–269] This is also superimposed on the complex phase behavior of Li-conductors depending on lithium concentration,[60,265,267,268,270] formation of dendrites,[47,49,271] *etc.* Therefore, to minimize the unwanted chemical stress effects, the components and microstructure of solid-state batteries need to be optimized with respect to chemical expansion.[47,60,263,272] To achieve the necessary degree of optimization, several important aspects should be taken into account, among which are the compressibility of the battery components, the extent of pore filling due to volume changes, the morphology of the electrodes, *etc.*[48,60,263] A very good example of this kind of optimization was shown by Koerver *et al.*[60] where the authors combined two compounds with negative and positive chemical expansion to obtain an active electrode material with almost no chemical strain.

Unfortunately, this elegant method of avoiding chemical strain seems to be completely inapplicable in case of oxide materials for SOFCs since oxygen release, *i.e.* reduction, never leads to significant volume contraction, at least for the known oxide materials. However, as discussed above, oxides with an anisotropic (for example, layered) crystal structure may possess negative chemical lattice strain along some selected crystallographic directions.[31,123,144,148,149,226–235,256–258] This decreases the overall volume chemical expansion compared to similar isotropic oxide materials. Therefore, it is logical to assume that in some materials with an appropriately selected crystal structure and chemical composition, ideal compensation of chemical expansion and contraction, occurring simultaneously in different crystallographic directions, can be achieved. Kharton *et al.*[255] reported that this may indeed be observed, at least in the particular range of temperatures and oxygen partial pressures, in the case of $Sr_3Fe_{2-x}Mo_xO_{7-\delta}$ oxides showing almost zero volumetric chemical expansion. Hence, controlling the lattice anisotropy through variation of an oxide's chemical composition and crystal structure can be viewed as an effective way of engineering chemical expansion. In this respect, layered oxides belonging to Ruddlesden–Popper, Dion–Jacobson and other homologous series, relatively unexplored from the viewpoint of chemical expansion, offer great structural and defect chemical flexibility and seem to be good model objects for further study of chemical strain phenomena.

Although, as mentioned above, chemical expansion is usually considered as a drawback leading to many problems when designing solid state electrochemical devices, in some cases, it can be beneficial. For example, many perovskite-like SOFC materials are known to suffer from alkaline earth metal (Sr or Ba) segregation on their surface, which negatively impacts their electrochemical performance. Both experimental and computational data indicate that at least for some of them introducing additional tensile strain suppresses the detrimental segregation.[273] While applying external strain to a solid oxide electrochemical cell is impracticable, an effective internal strain can be created either at the synthesis stage, *e.g.*, by isovalent B-site doping or A-site substoichiometry, or using *operando* techniques, by applying a cathodic bias (*i.e.* lowering the p_{O_2}). The latter increases the oxygen nonstoichiometry, which simultaneously shifts the respective equilibria away from the SrO segregation and causes chemical strain that works to the same effect.[273,274] This opens the possibility of enhancing the stability of materials' interfaces by intentionally providing additional chemical-expansion-induced internal strain, while the undesirable side effects of chemical expansion, such as mechanical cracking, could be mitigated by other means, *e.g.*, by creating composite materials.

While the abovementioned example of how materials could benefit from chemical strain can be viewed as a fortunate side effect, a few ways of using chemical expansivity directly for analytical and engineering purposes have been discovered recently (see Fig. 10). For instance, Swallow *et al.*[170] demonstrated a proof of concept, shown in Fig. 10a, of how a "mechanical" part of mechano-electro-chemical coupling in nonstoichiometric oxides can be utilized. By applying bias voltages lower than 0.1 V (much less than would be necessary for similar piezoelectric actuators) to a $Ce_{0.9}Pr_{0.1}O_{2-\delta}$ thin film

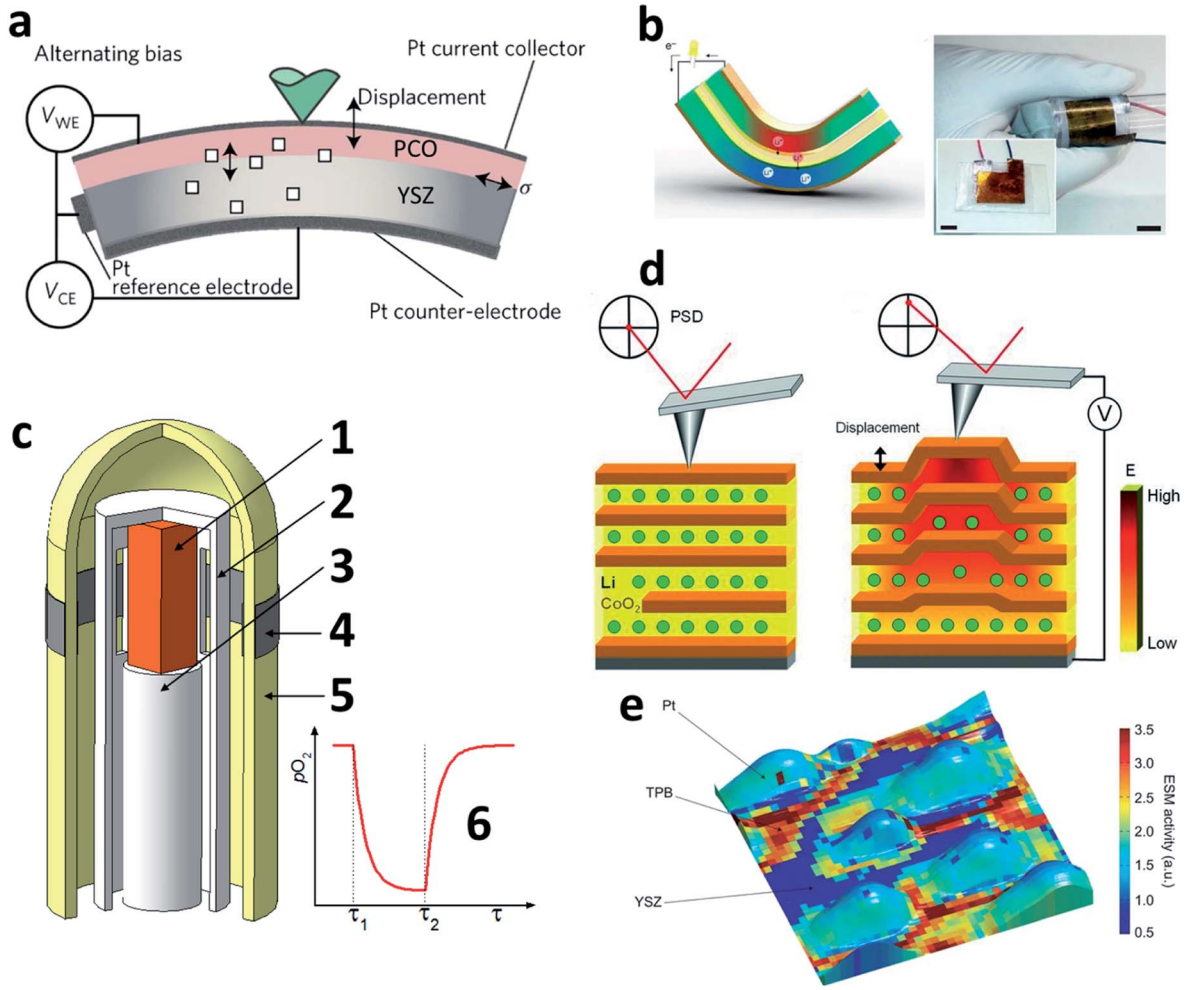

Fig. 10 (a) Illustration of the working principles of a thin film dynamic chemical expansion actuator: PCO – $Ce_{0.9}Pr_{0.1}O_{2-\delta}$, YSZ – yttria-stabilized zirconia. Adapted with permission from Springer Nature, J. G. Swallow, J. J. Kim, J. M. Maloney, D. Chen, J. F. Smith, S. R. Bishop, H. L. Tuller and K. J. Van Vliet, Dynamic chemical expansion of thin-film non-stoichiometric oxides at extreme temperatures, *Nat. Mater.*, 2017, **16**, 749–754, © 2017.[170] (b) A prototype of the mechanical energy harvester: (left) schematic view of the device design. The compressed region is illustrated in red while the tensile region is illustrated in blue. Lithium ions migrating from the compressed plate to the tensile plate are shown with arrows. The electrolyte soaked separator is drawn in yellow. (right) An image of the actual device with a bending unit. Both scale bars indicate 1 cm. Reprinted from S. Kim, S. J. Choi, K. Zhao, H. Yang, G. Gobbi, S. Zhang and J. Li, *Nat. Commun.*, 2016, **7**, 10146.[279] (c) Experimental apparatus for load-induced oxygen absorption measurements: 1 – oxide sample, 2 – sample holder, 3 – pushrod, 4 – YSZ electrolyte, 5 – Pt electrodes, 6 – typical p_{O_2} signal before ($\tau < \tau_1$) and after ($\tau_1 < \tau < \tau_2$) applying the load, and after releasing the load ($\tau > \tau_2$).[280] (d) Electromechanical response of a battery material due to the correlation between Li-ion concentration and molar volume. (left) The scanning probe microscope tip is in contact with the sample surface (shown in layered $LiCoO_2$ as an example). (right) Locally applied electrical fields result in Li-ion redistribution in the probed volume, which leads to surface displacements. PSD – position sensitive detector. Reproduced from S. V. Kalinin and N. Balke, *Adv. Mater.*, 2010, **22**, E193–E209, with permission from John Wiley and Sons, © 2010.[28] (e) Overlay of electrochemical activity on the topography of the nanoparticles revealing the enhancement of activity along the triple-phase boundaries (TPB). ESM – electrochemical strain microscopy. This surface segment is around 270 × 270 nm in size. Reprinted with permission from Springer Nature, A. Kumar, F. Ciucci, A. N. Morozovska, S. V. Kalinin and S. Jesse, Measuring oxygen reduction/evolution reactions on the nanoscale, *Nat. Chem.*, 2011, **3**, 707–713, © 2011.[291]

grown on a YSZ substrate, *i.e.* by electrochemically pumping oxygen into or out of the film, they achieved nanometer-scale displacement (>0.1% strain) at 650 °C.[173] Further developments of this approach[275] resulted in a MEC actuator prototype capable of micrometer-scale displacement at room temperature.[276] This actuator was made of a 150 nm thick $Ce_{0.8}Gd_{0.2}O_{1.9}$ electrolyte membrane sandwiched between two 100 nm thick composite $Ti/Ce_{0.8}Gd_{0.2}O_{1.9}$ electrodes, or working bodies, which provided mechanical action *via* their oxidation or reduction under the voltage applied.[276]

A somewhat different example of room-temperature strain engineering was reported by Manca *et al.*,[277] who adjusted the resonant frequency of WO_3 microresonators by hydrogen gas intercalation into the WO_3 crystal lattice. Thus, non-stoichiometric oxides with hydrogen- or oxygen-exchange-driven chemical strain capabilities could make a significant contribution to the emerging field of "straintronics".[278]

Another interesting feature of materials prone to chemical lattice strain stems from its reversibility and reciprocity: whereas the change in chemical composition can cause

mechanical strain, the reverse is also true, *i.e.* variation of chemical composition itself can be caused by applying external mechanical strain. Based on this phenomenon, Kim *et al.*[279] developed a device for mechano-electro-chemical energy harvesting, shown in Fig. 10b. The device consists of an electrolyte layer placed between two identical electrodes. The EMF between them, driving Li^+ ions from the compressed to the tensed electrode, is caused by the asymmetric stress applied to the device.[279] Though, in fact, Li-alloyed Si electrodes were used in the original work,[279] the working principle would be the same for oxide-based Li-conducting ones.

Likewise, the application of external mechanical strain to an oxide shifts its oxygen chemical potential and results in the readjustment of its equilibrium oxygen content. Some illustrative experiments in this respect were reported by Gerbshtein *et al.*,[280] who applied the load to a bulk $YBa_2Cu_3O_{6+\delta}$ sample under different external conditions (T, p_{O_2}). Fig. 10c shows a sketch of the setup as well as a typical p_{O_2} sensor response curve. As seen, compression leads to a p_{O_2} decrease due to the oxygen absorption by the sample, while the release of the load results in oxygen desorption, returning the whole system to the initial (mechanically unloaded) equilibrium state. The change of oxygen chemical potential per unit load as a function of oxygen content in $YBa_2Cu_3O_{6+\delta}$, obtained by Gerbshtein *et al.*,[280] was found to correlate well with the thermodynamics of oxygen exchange and existence of phase transitions in this oxide, making this method an interesting, though somewhat exotic, analytical technique.

In thin films, misfit epitaxial strain may also play the role of an external mechanical load and, hence, can be employed to modify the oxygen content and related properties of the film. For example, Petrie *et al.*[281] showed that controlling epitaxial strain in $SrCoO_{3-\delta}$ thin films allows oxygen deficiencies in the cobaltite to be tailored from $\delta \leq 0.1$ to $\delta \sim 0.25$ in aqueous, highly oxidizing environments. These shifts in the oxygen content occur through modest amounts of tensile strain, around 1–4%, resulting in anion concentrations unattainable in the unstrained bulk material. In turn, the additional oxygen vacancies created through tensile strain enhance the catalytic activity of $SrCoO_{3-\delta}$ toward the oxygen evolution reaction by over an order of magnitude, equaling that of precious-metal catalysts such as IrO_2.[281]

The reverse is also true, *i.e.* chemical deformation due to targeted change of the oxygen content in the strained film can serve as a strain mediation mechanism.[168,282–284] However, in case of thin films as compared to bulk samples the situation is complicated by anisotropic lattice distortions around oxygen vacancies inherent to many ABO_3 perovskites.[173,174] Elastic interactions of vacancy dipoles with an epitaxial misfit strain lead to preferential location of oxygen vacancies in a definite type of atomic plane and, as a result, may cause vacancy ordering, formation of new phases, or phase coexistence/separation.[174] In turn, this may alter the charge transfer properties and cause many other side effects.[173,174,285] To control them, the microscopic nature and elastic behavior of oxygen vacancies in epitaxial films should be thoroughly studied by both experimental and computational techniques.

On the nanoscale, chemical strain is used as a working principle of some modern microscopic techniques such as, for example, electrochemical strain microscopy (ESM).[27,286–288] This is a scanning probe microscopy (SPM) related method, which is based on the detection of electrochemical strain associated with ionic movement during a local redox process induced by electrochemical polarization of the cantilever's tip. Fig. 10d demonstrates how such an electromechanical response originates.[28] This allows direct study of redox reactions on the nanometer scale providing insights into both their kinetics and thermodynamics.[286,289] The ESM technique was widely employed for investigation of both Li-ion[28,286,290] and oxide-ion[289,291] conducting materials. Fig. 10e shows, as an example, the results of mapping electrochemical activity near a triple-phase boundary on the platinum-nanoparticle-coated YSZ surface.[291]

7. Conclusions

Energy-related oxide materials are operated commonly at elevated temperatures in both oxidizing and reducing environments and undergo upon heating not only thermal expansion, but also chemical strain caused by a change in their oxygen content or by their hydration. This strain can be detrimental to the practical application of such materials; therefore, its understanding is a challenge critically affecting further progress in the development of energy conversion and storage devices. It explains why so many efforts regarding both experimental and theoretical studies of the chemical strain in the oxides were undertaken in the last few decades. Despite the great attention it has attracted, chemical strain remains far from being fully understood even for relatively simple – with respect to their crystal structure – fluorites and pseudocubic perovskites.

To date, approaches available to explain the phenomenon of chemical strain are either based on computationally expensive methods with multiple arbitrarily variable parameters or limited to qualitative reasoning and empirical expressions. The latter are mostly evaluated on the basis of geometric assumptions and are, therefore, associated mainly with the crystal but not with the defect structure of oxides. Such a disregard for the defect structure when discussing chemical expansion leads to the empirical models being applicable only for a limited number of oxide materials. As a result, these models rarely allow the reasonably accurate values of chemical deformation to be predicted without carrying out the experimental measurements of chemical expansion itself. Furthermore, the relationship between the nature of the host and dopant cations and the effective radius of the oxygen vacancy has long been considered of importance for understanding the nature of chemical strain in oxides. However, to date, neither extensive computations nor empirical model analysis has led to any definite agreement regarding the size and shape of the oxygen vacancy and their variability across oxides with different structures and compositions. Meanwhile, an alternative approach to chemical strain modeling – using the oxygen nonstoichiometry dependence of cation coordination number instead of estimating the oxygen vacancy radius – remains underdeveloped.

Some other challenges may be summarized as follows. First of all, there is a strong need to understand the influence of the particularities of the oxide local structure on the chemical expansion. This includes the variation of coordination environments of ionic species, formation of defect clusters, nanodomains embedded in the matrix of the main phase, *etc.* For example, recent studies of ceria solid solutions[97–104] show that all these aspects may significantly affect the behavior of the material including, of course, its chemical expansion. In this regard, it is clear that chemical strain should be reanalyzed with the emphasis on the real spatial arrangement of the constituent ionic species and not only on the idealized fluorite structure as was done in the past. This should be true for perovskite-type oxides as well.

The magnetic contribution to the chemical expansion mentioned above for some double perovskites[226–232,246] is another emerging field of study which may hold answers for some still unexplained chemical strain related phenomena. This is also true for anisotropic chemical expansion of layered oxide materials, which have not yet been studied extensively in this respect, but the existing body of knowledge[10,31,123,144,148,149,226–235,254,256,257,259] indicates that controlling the degree of anisotropy may be an important route to controlling the chemical expansion of oxides.

All in all, the field of chemical expansion as it develops will definitely have a profound impact on both our fundamental understanding of solid state materials and on our ability to design new oxide materials for their application in various energy-related devices.

Conflicts of interest

The authors declare no conflicts of interest.

Acknowledgements

Dmitry Malyshkin acknowledges the project MK-800.2020.3 supported by the Council on grants of the President of the Russian Federation. The authors are grateful for the financial aid of the Ministry of Science and Higher Education of the Russian Federation (State Assignment No. 075-03-2021-051/5).

References

1 T. Ishihara, *Perovskite Oxide for Solid Oxide Fuel Cells*, Springer, US, Boston, MA, 2009.
2 J. A. Kilner and M. Burriel, *Annu. Rev. Mater. Res.*, 2014, **44**, 365–393.
3 J. Sunarso, S. Baumann, J. M. Serra, W. A. Meulenberg, S. Liu, Y. S. Lin and J. C. Diniz da Costa, *J. Membr. Sci.*, 2008, **320**, 13–41.
4 M. Misono, in *Studies in Surface Science and Catalysis*, ed. M. Misono, Elsevier, 2013, vol. 176, pp. 67–95.
5 J. D. Nicholas, Y. Qi, S. R. Bishop and P. P. Mukherjee, *J. Electrochem. Soc.*, 2014, **161**, Y11–Y12.
6 V. V. Sereda, D. S. Tsvetkov, D. A. Malyshkin, I. L. Ivanov, A. L. Sednev-Lugovets and A. Y. Zuev, *Solid State Ionics*, 2020, **358**, 115516.
7 W. Zhang, D. Schröder, T. Arlt, I. Manke, R. Koerver, R. Pinedo, D. A. Weber, J. Sann, W. G. Zeier and J. Janek, *J. Mater. Chem. A*, 2017, **5**, 9929–9936.
8 L. Mu, R. Lin, R. Xu, L. Han, S. Xia, D. Sokaras, J. D. Steiner, T.-C. Weng, D. Nordlund, M. M. Doeff, Y. Liu, K. Zhao, H. L. Xin and F. Lin, *Nano Lett.*, 2018, **18**, 3241–3249.
9 K.-J. Park, J.-Y. Hwang, H.-H. Ryu, F. Maglia, S.-J. Kim, P. Lamp, C. S. Yoon and Y.-K. Sun, *ACS Energy Lett.*, 2019, **4**, 1394–1400.
10 S. R. Bishop, D. Marrocchelli, C. Chatzichristodoulou, N. H. Perry, M. B. Mogensen, H. L. Tuller and E. D. Wachsman, *Annu. Rev. Mater. Res.*, 2014, **44**, 205–239.
11 S. Hull, S. T. Norberg, I. Ahmed, S. G. Eriksson, D. Marrocchelli and P. A. Madden, *J. Solid State Chem.*, 2009, **182**, 2815–2821.
12 D. Marrocchelli, S. R. Bishop, H. L. Tuller and B. Yildiz, *Adv. Funct. Mater.*, 2012, **22**, 1958–1965.
13 V. V. Sereda, D. S. Tsvetkov, I. L. Ivanov and A. Y. Zuev, *Acta Mater.*, 2019, **162**, 33–45.
14 M. B. Choi, S. Y. Jeon, H. S. Yang, J. Y. Park and S. J. Song, *J. Electrochem. Soc.*, 2011, **158**, B189.
15 M. B. Choi, D. K. Lim, E. D. Wachsman and S. J. Song, *Solid State Ionics*, 2012, **221**, 22–27.
16 H. Im, S. Jeon, M. Choi, J. Park and S. Song, *J. Ceram. Process. Res.*, 2012, **13**, 579–585.
17 A. Y. Zuev, V. Sereda and D. Tsvetkov, *Int. J. Hydrogen Energy*, 2014, **39**, 21553–21560.
18 A. Y. Zuev, V. Sereda and D. Tsvetkov, *J. Electrochem. Soc.*, 2014, **161**, F3032–F3038.
19 H. Bae, B. Singh, I.-H. Kim, H.-N. Im and S.-J. Song, *J. Electrochem. Soc.*, 2018, **165**, F641–F651.
20 H. Bae, J. Hong, B. Singh, A. K. Srivastava, J. H. Joo and S.-J. Song, *J. Electrochem. Soc.*, 2019, **166**, F180–F189.
21 D. Marrocchelli, S. R. Bishop and J. Kilner, *J. Mater. Chem. A*, 2013, **1**, 7673–7680.
22 H. Wulfmeier, D. Kohlmann, T. Defferriere, C. Steiner, R. Moos, H. L. Tuller and H. Fritze, *Z. Phys. Chem.*, 2021, DOI: 10.1515/zpch-2021-3125.
23 A. Y. Zuev and D. S. Tsvetkov, in *Electro-Chemo-Mechanics of Solids*, ed. S. R. Bishop, N. H. Perry, D. Marrocchelli and B. W. Sheldon, Springer International Publishing, Cham, 2017, pp. 5–33, DOI: 10.1007/978-3-319-51407-9_2.
24 Y.-D. Kim, J. Yang, J.-I. Lee, M. Saqib, J.-S. Shin, K. Park, M. Jo, S.-J. Song and J.-Y. Park, *J. Power Sources*, 2020, **452**, 227758.
25 H.-H. Ryu, K.-J. Park, C. S. Yoon and Y.-K. Sun, *Chem. Mater.*, 2018, **30**, 1155–1163.
26 J. H. Jang, Y.-M. Kim, Q. He, R. Mishra, L. Qiao, M. D. Biegalski, A. R. Lupini, S. T. Pantelides, S. J. Pennycook, S. V. Kalinin and A. Y. Borisevich, *ACS Nano*, 2017, **11**, 6942–6949.
27 N. Balke, S. Jesse, Y. Kim, L. Adamczyk, I. N. Ivanov, N. J. Dudney and S. V. Kalinin, *ACS Nano*, 2010, **4**, 7349–7357.

28 S. V. Kalinin and N. Balke, *Adv. Mater.*, 2010, **22**, E193–E209.
29 J. Li, Y. Li, P. K. Routh, E. Makagon, I. Lubomirsky and A. I. Frenkel, *J. Synchrotron Radiat.*, 2021, **28**, 1511–1517.
30 E. Sediva, T. Defferriere, N. H. Perry, H. L. Tuller and J. L. M. Rupp, *Adv. Mater.*, 2019, **31**, 1902493.
31 A. Chatterjee, J. M. Caicedo, B. Ballesteros and J. Santiso, *J. Mater. Chem. A*, 2018, **6**, 12430–12439.
32 D. Marrocchelli, N. H. Perry and S. R. Bishop, *Phys. Chem. Chem. Phys.*, 2015, **17**, 10028–10039.
33 D. S. Aidhy, B. Liu, Y. Zhang and W. J. Weber, *Comput. Mater. Sci.*, 2015, **99**, 298–305.
34 A. Løken, R. Haugsrud and T. S. Bjørheim, *Phys. Chem. Chem. Phys.*, 2016, **18**, 31296–31303.
35 B. Euser, J. R. Berger, H. Zhu and R. J. Kee, *J. Electrochem. Soc.*, 2016, **163**, F1294–F1301.
36 B. Euser, J. R. Berger, H. Zhu and R. J. Kee, *J. Electrochem. Soc.*, 2016, **163**, F264–F271.
37 N. Nagendra, S. Biswas, T. Nithyanantham and S. Bandopadhyay, *Mater. Res. Bull.*, 2013, **48**, 2034–2039.
38 A. Atkinson and T. M. G. M. Ramos, *Solid State Ionics*, 2000, **129**, 259–269.
39 K. Kwok, H. L. Frandsen, M. Søgaard and P. V. Hendriksen, *J. Membr. Sci.*, 2014, **470**, 80–89.
40 B. Euser, H. Zhu, J. R. Berger, C. A. Lewinsohn and R. J. Kee, *J. Electrochem. Soc.*, 2017, **164**, F732–F739.
41 E. Blond and N. Richet, *J. Eur. Ceram. Soc.*, 2008, **28**, 793–801.
42 K. Taghikhani, A. Dubois, J. R. Berger, S. Ricote, H. Zhu and R. J. Kee, *Membranes*, 2021, **11**, 378.
43 X. Jin and X. Xue, *RSC Adv.*, 2014, **4**, 15782–15796.
44 Y. Wu, X. Xu, Z. Yan and Z. Zhong, *J. Electrochem. Soc.*, 2021, **168**, 044511.
45 S. R. Bishop, *Acta Mech. Sin.*, 2013, **29**, 312–317.
46 A. Løken, S. Ricote and S. Wachowski, *Crystals*, 2018, **8**, 365.
47 P. Wang, W. Qu, W.-L. Song, H. Chen, R. Chen and D. Fang, *Adv. Funct. Mater.*, 2019, **29**, 1900950.
48 Y. Ren and K. B. Hatzell, *J. Mater. Chem. A*, 2021, **9**, 13804–13821.
49 J. A. Lewis, J. Tippens, F. J. Q. Cortes and M. T. McDowell, *Trends Chem.*, 2019, **1**, 845–857.
50 Y. Wang, J. Liu, T. Chen, W. Lin and J. Zheng, *Phys. Chem. Chem. Phys.*, 2022, **24**, 2167–2175.
51 D. Bistri, A. Afshar and C. V. Di Leo, *Meccanica*, 2021, **56**, 1523–1554.
52 Z. Xu, M. M. Rahman, L. Mu, Y. Liu and F. Lin, *J. Mater. Chem. A*, 2018, **6**, 21859–21884.
53 Y. S. Touloukian, R. K. Kirby, E. R. Taylor and T. Y. R. Lee, *Thermophysical Properties of Matter - The TPRC Data Series. Volume 13. Thermal Expansion - Nonmetallic Solids*, IFI/Plenum Data Company, New York, 1977.
54 R. S. Krishnan, R. Srinivasan and S. Devanarayanan, *Thermal Expansion of Crystals*, Pergamon Press, Oxford, 1979.
55 P. G. Strelkow, *Phys. Z. Sowjetunion*, 1937, **12**, 77–82.
56 N. F. Mott and R. W. Gurney, *Electronic Processes in Ionic Crystals*, Clarendon Press, Oxford, 1948.
57 F. Seitz, *Phys. Rev.*, 1939, **56**, 1063–1064.
58 A. W. Lawson, *Phys. Rev.*, 1950, **78**, 185.
59 E. R. Jette and F. Foote, *J. Chem. Phys.*, 1933, **1**, 29–36.
60 R. Koerver, W. Zhang, L. de Biasi, S. Schweidler, A. O. Kondrakov, S. Kolling, T. Brezesinski, P. Hartmann, W. G. Zeier and J. Janek, *Energy Environ. Sci.*, 2018, **11**, 2142–2158.
61 D. Marrocchelli, C. Chatzichristodoulou and S. R. Bishop, *Phys. Chem. Chem. Phys.*, 2014, **16**, 9229–9232.
62 S. B. Adler, *J. Am. Ceram. Soc.*, 2001, **84**, 2117–2119.
63 A. Løken, S. Ricote and S. Wachowski, *Crystals*, 2018, 8.
64 T. S. Bjørheim, A. Løken and R. Haugsrud, *J. Mater. Chem. A*, 2016, **4**, 5917–5924.
65 V. Tsidilkovski, A. Kuzmin, L. Putilov and V. Balakireva, *Solid State Ionics*, 2017, **301**, 170–175.
66 T. Fujisaki, A. T. Staykov, Y. Jing, K. Leonard, N. R. Aluru and H. Matsumoto, *Solid State Ionics*, 2019, **333**, 1–8.
67 A. K. E. Andersson, S. M. Selbach, C. S. Knee and T. Grande, *J. Am. Ceram. Soc.*, 2014, **97**, 2654–2661.
68 D. Han, N. Hatada and T. Uda, *J. Am. Ceram. Soc.*, 2016, **99**, 3745–3753.
69 R. Sažinas, M.-A. Einarsrud and T. Grande, *J. Mater. Chem. A*, 2017, **5**, 5846–5857.
70 E. Jedvik, A. Lindman, M. Þ. Benediktsson and G. Wahnström, *Solid State Ionics*, 2015, **275**, 2–8.
71 C. Chatzichristodoulou, P. Norby, P. V. Hendriksen and M. B. Mogensen, *J. Electroceram.*, 2015, **34**, 100–107.
72 S. J. Hong and A. V. Virkar, *J. Am. Ceram. Soc.*, 1995, **78**, 433–439.
73 V. B. Glushkova, F. Hanic and L. V. Sazonova, *Ceramurg. Int.*, 1978, **4**, 176–178.
74 R. P. Ingel and D. Lewis, *J. Am. Ceram. Soc.*, 1986, **69**, 325–332.
75 V. I. Aleksandrov, G. E. Val'yano, B. V. Lukin, V. V. Osiko, A. E. Rautbort, V. M. Tatarintsev and V. N. Filatova, 1976, **12**, 273–277.
76 D.-J. Kim, *J. Am. Ceram. Soc.*, 1989, **72**, 1415–1421.
77 S. Omar and J. C. Nino, *Acta Mater.*, 2013, **61**, 5406–5413.
78 L. Vegard, *Z. Phys.*, 1921, **5**, 17–26.
79 A. N. Morozovska, E. A. Eliseev, G. S. Svechnikov and S. V. Kalinin, *Phys. Rev. B: Condens. Matter Mater. Phys.*, 2011, **84**, 045402.
80 N. Balke, S. Jesse, A. N. Morozovska, E. Eliseev, D. W. Chung, Y. Kim, L. Adamczyk, R. E. García, N. Dudney and S. V. Kalinin, *Nat. Nanotechnol.*, 2010, **5**, 749–754.
81 R. Shannon, *Acta Crystallogr. A*, 1976, **32**, 751–767.
82 M. Mogensen, N. M. Sammes and G. A. Tompsett, *Solid State Ionics*, 2000, **129**, 63–94.
83 T. Otake, H. Yugami, K. Yashiro, Y. Nigara, T. Kawada and J. Mizusaki, *Solid State Ionics*, 2003, **161**, 181–186.
84 S. R. Bishop, K. L. Duncan and E. D. Wachsman, *Electrochim. Acta*, 2009, **54**, 1436–1443.
85 S. R. Bishop, H. L. Tuller, Y. Kuru and B. Yildiz, *J. Eur. Ceram. Soc.*, 2011, **31**, 2351–2356.
86 S. R. Bishop, D. Marrocchelli, W. Fang, K. Amezawa, K. Yashiro and G. W. Watson, *Energy Environ. Sci.*, 2013, **6**, 1142–1146.

87 S. R. Bishop, T. Nakamura and K. Amezawa, *Solid State Ionics*, 2014, **261**, 1–4.
88 D. Er, J. Li, M. Cargnello, P. Fornasiero, R. J. Gorte and V. B. Shenoy, *J. Electrochem. Soc.*, 2014, **161**, F3060–F3064.
89 B. Wang, X. Xi and A. N. Cormack, *Chem. Mater.*, 2014, **26**, 3687–3692.
90 M. Heidenreich, C. Kaps, A. Simon, F. Schulze-Küppers and S. Baumann, *Solid State Ionics*, 2015, **283**, 56–67.
91 T. Das, J. D. Nicholas, B. W. Sheldon and Y. Qi, *Phys. Chem. Chem. Phys.*, 2018, **20**, 15293–15299.
92 H.-W. Chiang, R. N. Blumenthal and R. A. Fournelle, *Solid State Ionics*, 1993, **66**, 85–95.
93 S. Wang, M. Katsuki, T. Hashimoto and M. Dokiya, *J. Electrochem. Soc.*, 2003, **150**, A952.
94 S. R. Bishop, K. L. Duncan and E. D. Wachsman, *Acta Mater.*, 2009, **57**, 3596–3605.
95 A. Nakamura, *Solid State Ionics*, 2010, **181**, 1543–1564.
96 A. Nakamura, *Solid State Ionics*, 2010, **181**, 1631–1653.
97 C. Artini, M. Pani, M. M. Carnasciali, M. T. Buscaglia, J. R. Plaisier and G. A. Costa, *Inorg. Chem.*, 2015, **54**, 4126–4137.
98 C. Artini, M. Pani, M. M. Carnasciali, J. R. Plaisier and G. A. Costa, *Inorg. Chem.*, 2016, **55**, 10567–10579.
99 C. Artini, *Inorg. Chem.*, 2018, **57**, 13047–13062.
100 C. Artini, M. M. Carnasciali, M. Viviani, S. Presto, J. R. Plaisier, G. A. Costa and M. Pani, *Solid State Ionics*, 2018, **315**, 85–91.
101 C. Artini, S. Presto, S. Massardo, M. Pani, M. M. Carnasciali and M. Viviani, *Energies*, 2019, **12**, 4148.
102 C. Artini, S. Massardo, M. M. Carnasciali, B. Joseph and M. Pani, *Inorg. Chem.*, 2021, **60**, 7306–7314.
103 C. Artini, S. Presto, M. Viviani, S. Massardo, M. M. Carnasciali, L. Gigli and M. Pani, *J. Energy Chem.*, 2021, **60**, 494–502.
104 S. Massardo, A. Cingolani and C. Artini, *Coatings*, 2021, **11**, 724.
105 M. Johnsson and P. Lemmens, in *Handbook of Magnetism and Advanced Magnetic Materials*, Wiley, Hoboken, 2007, pp. 2034–2042, DOI: 10.1002/9780470022184.hmm411.
106 V. L. Miller and S. C. Tidrow, *Integr. Ferroelectr.*, 2013, **148**, 1–16.
107 X. Chen and T. Grande, *Chem. Mater.*, 2013, **25**, 927–934.
108 X. Chen and T. Grande, *Chem. Mater.*, 2013, **25**, 3296–3306.
109 T. Grande, J. R. Tolchard and S. M. Selbach, *Chem. Mater.*, 2012, **24**, 338–345.
110 S. M. Selbach, A. Nordli Løvik, K. Bergum, J. R. Tolchard, M.-A. Einarsrud and T. Grande, *J. Solid State Chem.*, 2012, **196**, 528–535.
111 N. H. Perry, S. R. Bishop and H. L. Tuller, *J. Mater. Chem. A*, 2014, **2**, 18906–18916.
112 N. H. Perry, J. J. Kim, S. R. Bishop and H. L. Tuller, *J. Mater. Chem. A*, 2015, **3**, 3602–3611.
113 L. Q. Jiang, J. K. Guo, H. B. Liu, M. Zhu, X. Zhou, P. Wu and C. H. Li, *J. Phys. Chem. Solids*, 2006, **67**, 1531–1536.
114 T. R. Armstrong, J. W. Stevenson, L. R. Pederson and P. E. Raney, *J. Electrochem. Soc.*, 1996, **143**, 2919–2925.
115 P. H. Larsen, P. V. Hendriksen and M. Mogensen, *J. Therm. Anal.*, 1997, **49**, 1263–1275.
116 S. Miyoshi, J.-O. Hong, K. Yashiro, A. Kaimai, Y. Nigara, K. Kawamura, T. Kawada and J. Mizusaki, *Solid State Ionics*, 2003, **161**, 209–217.
117 J. Mizusaki, N. Mori, H. Takai, Y. Yonemura, H. Minamiue, H. Tagawa, M. Dokiya, H. Inaba, K. Naraya, T. Sasamoto and T. Hashimoto, *Solid State Ionics*, 2000, **129**, 163–177.
118 Yu Chen and S. B. Adler, *Chem. Mater.*, 2005, **17**, 4537–4546.
119 A. Zuev, L. Singheiser and K. Hilpert, *Solid State Ionics*, 2002, **147**, 1–11.
120 K. Hilpert, R. W. Steinbrech, F. Boroomand, E. Wessel, F. Meschke, A. Zuev, O. Teller, H. Nickel and L. Singheiser, *J. Eur. Ceram. Soc.*, 2003, **23**, 3009–3020.
121 A. Y. Zuev, A. I. Vylkov, A. N. Petrov and D. S. Tsvetkov, *Solid State Ionics*, 2008, **179**, 1876–1879.
122 A. Y. Zuev and D. S. Tsvetkov, *Solid State Ionics*, 2010, **181**, 557–563.
123 D. S. Tsvetkov, I. L. Ivanov, D. Malyshkin, V. V. Sereda and A. Y. Zuev, *ECS Trans.*, 2016, **72**, 21–35.
124 Y.-L. Lee and D. Morgan, *Phys. Chem. Chem. Phys.*, 2012, **14**, 290–302.
125 S. Shafeie, J. Grins, S. Y. Istomin, A. A. Gippius, L. Karvonen, S. Populoh, A. Weidenkaff, J. Köhler and G. Svensson, *J. Mater. Chem.*, 2012, **22**, 16269–16276.
126 P. M. Raccah and J. B. Goodenough, *Phys. Rev.*, 1967, **155**, 932–943.
127 M. A. Señarís-Rodríguez and J. B. Goodenough, *J. Solid State Chem.*, 1995, **116**, 224–231.
128 M. W. Haverkort, Z. Hu, J. C. Cezar, T. Burnus, H. Hartmann, M. Reuther, C. Zobel, T. Lorenz, A. Tanaka, N. B. Brookes, H. H. Hsieh, H. J. Lin, C. T. Chen and L. H. Tjeng, *Phys. Rev. Lett.*, 2006, **97**, 176405.
129 M. A. Señarís-Rodríguez and J. B. Goodenough, *J. Solid State Chem.*, 1995, **118**, 323–336.
130 C. Zobel, M. Kriener, D. Bruns, J. Baier, M. Grüninger, T. Lorenz, P. Reutler and A. Revcolevschi, *Phys. Rev. B: Condens. Matter Mater. Phys.*, 2002, **66**, 020402.
131 X. Wang, Y. Han, X. Song, W. Liu, Y. Jin, W. Liu and H. Cui, *Phys. Chem. Chem. Phys.*, 2018, **20**, 17781–17789.
132 S. Y. Istomin and E. V. Antipov, *Russ. Chem. Rev.*, 2013, **82**, 686–700.
133 A. Y. Zuev, V. V. Sereda and D. S. Tsvetkov, *J. Electrochem. Soc.*, 2012, **159**, F594–F599.
134 M.-B. Choi, S.-Y. Jeon, B. Singh, Y.-S. Yoo, J.-H. Hwang and S.-J. Song, *Acta Mater.*, 2014, **65**, 373–382.
135 V. V. Sereda, D. S. Tsvetkov, I. L. Ivanov and A. Y. Zuev, *J. Mater. Chem. A*, 2015, **3**, 6028–6037.
136 Y. Takeda, K. Kanno, T. Takada, O. Yamamoto, M. Takano, N. Nakayama and Y. Bando, *J. Solid State Chem.*, 1986, **63**, 237–249.
137 T. C. Gibb, *J. Mater. Chem.*, 1994, **4**, 1445–1449.
138 J. P. Hodges, S. Short, J. D. Jorgensen, X. Xiong, B. Dabrowski, S. M. Mini and C. W. Kimball, *J. Solid State Chem.*, 2000, **151**, 190–209.
139 M. Schmidt and S. J. Campbell, *J. Solid State Chem.*, 2001, **156**, 292–304.
140 J. Blasco, J. Stankiewicz and J. García, *J. Solid State Chem.*, 2006, **179**, 898–908.

141 N. Kim, N. H. Perry and E. Ertekin, *Chem. Mater.*, 2019, **31**, 233–243.
142 B. Ouyang, T. Chakraborty, N. Kim, N. H. Perry, T. Mueller, N. R. Aluru and E. Ertekin, *Chem. Mater.*, 2019, **31**, 3144–3153.
143 T. Das, J. D. Nicholas and Y. Qi, *J. Mater. Chem. A*, 2017, **5**, 25031–25043.
144 D. S. Tsvetkov, I. L. Ivanov, D. A. Malyshkin and A. Y. Zuev, *Dalton Trans.*, 2014, **43**, 11862–11866.
145 D. S. Tsvetkov, I. L. Ivanov, D. A. Malyshkin, A. L. Sednev, V. V. Sereda and A. Y. Zuev, *Pure Appl. Chem.*, 2019, **91**, 923–940.
146 D. S. Tsvetkov, I. L. Ivanov, D. A. Malyshkin, A. S. Steparuk and A. Y. Zuev, *Dalton Trans.*, 2016, **45**, 12906–12913.
147 V. S. Kudyakova, A. M. Shalamova, B. V. Politov and A. Y. Suntsov, *J. Alloys Compd.*, 2021, **886**, 161133.
148 R. A. Cox-Galhotra, A. Huq, J. P. Hodges, J.-H. Kim, C. Yu, X. Wang, A. J. Jacobson and S. McIntosh, *J. Mater. Chem. A*, 2013, **1**, 3091–3100.
149 R. A. Cox-Galhotra, A. Huq, J. P. Hodges, C. Yu, X. Wang, W. Gong, A. J. Jacobson and S. McIntosh, *Solid State Ionics*, 2013, **249–250**, 34–40.
150 K. Papathanassopoulos, H. Wenzl and T. Schober, *J. Am. Ceram. Soc.*, 1997, **80**, 3278–3280.
151 T. Schober, J. Friedrich, D. Triefenbach and F. Tietz, *Solid State Ionics*, 1997, **100**, 173–181.
152 T. Mono and T. Schober, *Solid State Ionics*, 1996, **91**, 155–159.
153 K. D. Kreuer, *Annu. Rev. Mater. Res.*, 2003, **33**, 333–359.
154 E. Makagon, R. Merkle, J. Maier and I. Lubomirsky, *Solid State Ionics*, 2020, **344**, 115130.
155 D. Han, K. Shinoda, S. Sato, M. Majima and T. Uda, *J. Mater. Chem. A*, 2015, **3**, 1243–1250.
156 I. Ahmed, M. Karlsson, S.-G. Eriksson, E. Ahlberg, C. S. Knee, K. Larsson, A. K. Azad, A. Matic and L. Börjesson, *J. Am. Ceram. Soc.*, 2008, **91**, 3039–3044.
157 I. Oikawa and H. Takamura, *Chem. Mater.*, 2015, **27**, 6660–6667.
158 J. Hyodo, K. Kitabayashi, K. Hoshino, Y. Okuyama and Y. Yamazaki, *Adv. Energy Mater.*, 2020, **10**, 2000213.
159 A. V. Kasyanova, L. R. Tarutina, A. O. Rudenko, J. G. Lyagaeva and D. A. Medvedev, *Russ. Chem. Rev.*, 2020, **89**, 667–692.
160 D. Han, M. Majima and T. Uda, *J. Solid State Chem.*, 2013, **205**, 122–128.
161 A. V. Kuz'min, A. Y. Stroeva, V. P. Gorelov and A. A. Pankratov, *Russ. J. Electrochem.*, 2018, **54**, 43–48.
162 H. Xu, R. K. Behera, Y. Wang, F. Ebrahimi, S. B. Sinnott, E. D. Wachsman and S. R. Phillpot, *Solid State Ionics*, 2010, **181**, 551–556.
163 D. A. Freedman, D. Roundy and T. A. Arias, *Phys. Rev. B: Condens. Matter Mater. Phys.*, 2009, **80**, 064108.
164 S. J. Stokes and M. S. Islam, *J. Mater. Chem.*, 2010, **20**, 6258–6264.
165 M. Burbano, D. Marrocchelli, B. Yildiz, H. L. Tuller, S. T. Norberg, S. Hull, P. A. Madden and G. W. Watson, *J. Phys.: Condens. Matter*, 2011, **23**, 255402.
166 D. Marrocchelli, S. R. Bishop, H. L. Tuller, G. W. Watson and B. Yildiz, *Phys. Chem. Chem. Phys.*, 2012, **14**, 12070–12074.
167 E. J. Granhed, A. Lindman, C. Eklöf-Österberg, M. Karlsson, S. F. Parker and G. Wahnström, *J. Mater. Chem. A*, 2019, **7**, 16211–16221.
168 A. Marthinsen, T. Grande and S. M. Selbach, *J. Phys. Chem. C*, 2020, **124**, 12922–12932.
169 U. Aschauer and N. A. Spaldin, *Appl. Phys. Lett.*, 2016, **109**, 031901.
170 J. G. Swallow, J. J. Kim, J. M. Maloney, D. Chen, J. F. Smith, S. R. Bishop, H. L. Tuller and K. J. Van Vliet, *Nat. Mater.*, 2017, **16**, 749–754.
171 D. S. Aidhy and K. Rawat, *J. Appl. Phys.*, 2021, **129**, 171102.
172 J. Sheth, D. Chen, J. J. Kim, W. J. Bowman, P. A. Crozier, H. L. Tuller, S. T. Misture, S. Zdzieszynski, B. W. Sheldon and S. R. Bishop, *Nanoscale*, 2016, **8**, 16499–16510.
173 J. G. Swallow, J. K. Lee, T. Defferriere, G. M. Hughes, S. N. Raja, H. L. Tuller, J. H. Warner and K. J. Van Vliet, *ACS Nano*, 2018, **12**, 1359–1372.
174 M. Tyunina, O. Pacherova, T. Kocourek and A. Dejneka, *Sci. Rep.*, 2021, **11**, 15247.
175 X. Liu, L. Zhang, Y. Zheng, Z. Guo, Y. Zhu, H. Chen, F. Li, P. Liu, B. Yu, X. Wang, J. Liu, Y. Chen and M. Liu, *Adv. Sci.*, 2019, **6**, 1801898.
176 M. Kubicek, Z. Cai, W. Ma, B. Yildiz, H. Hutter and J. Fleig, *ACS Nano*, 2013, **7**, 3276–3286.
177 M. F. Hoedl, D. Gryaznov, R. Merkle, E. A. Kotomin and J. Maier, *J. Phys. Chem. C*, 2020, **124**, 11780–11789.
178 M. Ram and Y. Tsur, *J. Electroceram.*, 2009, **22**, 120–124.
179 C. S. Kim, N. H. Perry, S. R. Bishop and H. L. Tuller, *J. Electroceram.*, 2018, **40**, 332–337.
180 C. Chatzichristodoulou, P. V. Hendriksen and A. Hagen, *J. Electrochem. Soc.*, 2010, **157**, B299.
181 A. Natoli, B. I. Arias-Serrano, E. Rodríguez-Castellón, A. Żurawska, J. R. Frade and A. A. Yaremchenko, *Materials*, 2021, **14**, 641.
182 S. Wang, E. Oikawa and T. Hashimoto, *J. Electrochem. Soc.*, 2004, **151**, E46.
183 Y. Li, E. R. Maxey, J. W. Richardson Jr, B. Ma, T. H. Lee and S.-J. Song, *J. Am. Ceram. Soc.*, 2007, **90**, 1208–1214.
184 M. Kuhn, S. R. Bishop, J. L. M. Rupp and H. L. Tuller, *Acta Mater.*, 2013, **61**, 4277–4288.
185 T. R. Armstrong, J. W. Stevenson, K. Hasinska and D. E. McCready, *J. Electrochem. Soc.*, 1998, **145**, 4282–4289.
186 F. Boroomand, E. Wessel, H. Bausinger and K. Hilpert, *Solid State Ionics*, 2000, **129**, 251–258.
187 J. H. Kuo, H. U. Anderson and D. M. Sparlin, *J. Solid State Chem.*, 1989, **83**, 52–60.
188 S. Miyoshi, J.-O. Hong, K. Yashiro, A. Kaimai, Y. Nigara, K. Kawamura, T. Kawada and J. Mizusaki, *Solid State Ionics*, 2002, **154–155**, 257–263.
189 S. Miyoshi, A. Kaimai, H. Matsumoto, K. Yashiro, Y. Nigara, T. Kawada and J. Mizusaki, *Solid State Ionics*, 2004, **175**, 383–386.
190 J. A. M. Van Roosmalen, E. H. P. Cordfunke, R. B. Helmholdt and H. W. Zandbergen, *J. Solid State Chem.*, 1994, **110**, 100–105.
191 M. H. R. Lankhorst and H. J. M. Bouwmeester, *J. Electrochem. Soc.*, 1997, **144**, 1268–1273.

192 M. H. R. Lankhorst, H. J. M. Bouwmeester and H. Verweij, *J. Solid State Chem.*, 1997, **133**, 555–567.
193 M. H. R. Lankhorst, H. J. M. Bouwmeester and H. Verweij, *Solid State Ionics*, 1997, **96**, 21–27.
194 M. H. R. Lankhorst and J. E. ten Elshof, *J. Solid State Chem.*, 1997, **130**, 302–310.
195 V. Cherepanov, T. Aksenova, E. Kiselev and L. Gavrilova, *Solid State Sci.*, 2008, **10**, 438–443.
196 A. N. Petrov, V. A. Cherepanov and A. Y. Zuev, *J. Solid State Electrochem.*, 2006, **10**, 517–537.
197 A. Y. Zuev, A. N. Petrov, A. I. Vylkov and D. S. Tsvetkov, *J. Mater. Sci.*, 2007, **42**, 1901–1908.
198 M. Kuhn, S. Hashimoto, K. Sato, K. Yashiro and J. Mizusaki, *Solid State Ionics*, 2011, **195**, 7–15.
199 S. Wang, M. Katsuki, M. Dokiya and T. Hashimoto, *Solid State Ionics*, 2003, **159**, 71–78.
200 L. W. Tai, M. M. Nasrallah, H. U. Anderson, D. M. Sparlin and S. R. Sehlin, *Solid State Ionics*, 1995, **76**, 273–283.
201 C. Y. Park and A. J. Jacobson, *Solid State Ionics*, 2005, **176**, 2671–2676.
202 A. L. Allred and E. G. Rochow, *J. Inorg. Nucl. Chem.*, 1958, **5**, 264–268.
203 P. Hjalmarsson, M. Søgaard and M. Mogensen, *J. Solid State Chem.*, 2010, **183**, 1853–1862.
204 V. V. Kharton, A. A. Yaremchenko, M. V. Patrakeev, E. N. Naumovich and F. M. B. Marques, *J. Eur. Ceram. Soc.*, 2003, **23**, 1417–1426.
205 R. Kriegel, R. Kircheisen and J. Töpfer, *Solid State Ionics*, 2010, **181**, 64–70.
206 H. L. Lein, K. Wiik and T. Grande, *Solid State Ionics*, 2006, **177**, 1795–1798.
207 S. McIntosh, J. F. Vente, W. G. Haije, D. H. A. Blank and H. J. M. Bouwmeester, *Chem. Mater.*, 2006, **18**, 2187–2193.
208 X. Dong, Z. Xu, X. Chang, C. Zhang and W. Jin, *J. Am. Ceram. Soc.*, 2007, **90**, 3923–3929.
209 S. R. Bishop, K. L. Duncan and E. D. Wachsman, *J. Am. Ceram. Soc.*, 2010, **93**, 4115–4121.
210 A. Feldhoff, J. Martynczuk, M. Arnold, M. Myndyk, I. Bergmann, V. Šepelák, W. Gruner, U. Vogt, A. Hähnel and J. Woltersdorf, *J. Solid State Chem.*, 2009, **182**, 2961–2971.
211 M. G. Sahini, J. R. Tolchard, K. Wiik and T. Grande, *Dalton Trans.*, 2015, **44**, 10875–10881.
212 A. A. Yaremchenko, S. M. Mikhalev, E. S. Kravchenko and J. R. Frade, *J. Eur. Ceram. Soc.*, 2014, **34**, 703–715.
213 M. Kuhn, S. Hashimoto, K. Sato, K. Yashiro and J. Mizusaki, *Solid State Ionics*, 2013, **241**, 12–16.
214 S.-i. Hashimoto, Y. Fukuda, M. Kuhn, K. Sato, K. Yashiro and J. Mizusaki, *Solid State Ionics*, 2011, **186**, 37–43.
215 A. Fossdal, M. Menon, I. Wærnhus, K. Wiik, M.-A. Einarsrud and T. Grande, *J. Am. Ceram. Soc.*, 2004, **87**, 1952–1958.
216 C. de Leeuwe, W. Hu, D. Neagu, E. I. Papaioannou, S. Pramana, B. Ray, J. S. O. Evans and I. S. Metcalfe, *J. Solid State Chem.*, 2021, **293**, 121838.
217 H. Bae, B. Singh, L. Mathur, J. H. Joo and S.-J. Song, *J. Electrochem. Soc.*, 2021, **168**, 034511.
218 O. Valentin, F. Millot, É. Blond, N. Richet, A. Julian, E. Véron and S. Ory, *Solid State Ionics*, 2011, **193**, 23–31.
219 A. A. Yaremchenko, E. V. Tsipis, A. V. Kovalevsky, J. C. Waerenborgh and V. V. Kharton, *Solid State Ionics*, 2011, **192**, 259–268.
220 Y. Liu, S. Baumann, F. Schulze-Küppers, D. N. Mueller and O. Guillon, *J. Eur. Ceram. Soc.*, 2018, **38**, 5058–5066.
221 S. I. Elkalashy, T. V. Aksenova, A. S. Urusova and V. A. Cherepanov, *Solid State Ionics*, 2016, **295**, 96–103.
222 T. V. Aksenova, A. E. Vakhromeeva, S. I. Elkalashy, A. S. Urusova and V. A. Cherepanov, *J. Solid State Chem.*, 2017, **251**, 70–78.
223 A. M. Glazer, *Acta Crystallogr. B*, 1972, **28**, 3384–3392.
224 A. M. Glazer, *Acta Crystallogr. A*, 1975, **31**, 756–762.
225 G. King and P. M. Woodward, *J. Mater. Chem.*, 2010, **20**, 5785–5796.
226 P. Karen, *J. Solid State Chem.*, 2021, **299**, 122147.
227 P. Karen and P. M. Woodward, *J. Mater. Chem.*, 1999, **9**, 789–797.
228 P. Karen, P. M. Woodward, P. N. Santhosh, T. Vogt, P. W. Stephens and S. Pagola, *J. Solid State Chem.*, 2002, **167**, 480–493.
229 J. Lindén, P. Karen, A. Kjekshus, J. Miettinen, T. Pietari and M. Karppinen, *Phys. Rev. B: Condens. Matter Mater. Phys.*, 1999, **60**, 15251–15260.
230 J. Nakamura, J. Lindén, H. Yamauchi and M. Karppinen, *Solid State Commun.*, 2002, **121**, 269–274.
231 P. Karen, K. Gustafsson and J. Lindén, *J. Solid State Chem.*, 2007, **180**, 148–157.
232 P. Karen, *J. Solid State Chem.*, 2003, **170**, 9–23.
233 L. Mogni, F. Prado, C. Jiménez and A. Caneiro, *Solid State Ionics*, 2013, **240**, 19–28.
234 I. Szpunar, R. Strandbakke, M. H. Sørby, S. L. Wachowski, M. Balaguer, M. Tarach, J. M. Serra, A. Witkowska, E. Dzik, T. Norby, M. Gazda and A. Mielewczyk-Gryń, *Materials*, 2020, **13**, 4044.
235 A. L. Sednev-Lugovets, V. V. Sereda, D. A. Malyshkin, D. S. Tsvetkov, I. L. Ivanov, A. Y. Zuev and A. Maignan, *J. Chem. Therm.*, 2021, **161**, 106523.
236 C. Bernuy-Lopez, K. Høydalsvik, M.-A. Einarsrud and T. Grande, *Materials154-151&ndash*, 2016, **9**, 154–118.
237 D. A. Malyshkin, A. Y. Novikov, V. V. Sereda, I. L. Ivanov, D. S. Tsvetkov and A. Y. Zuev, *Inorg. Chem.*, 2018, **57**, 12409–12416.
238 D. Malyshkin, A. Novikov, D. Tsvetkov and A. Zuev, *Mater. Lett.*, 2018, **229**, 324–326.
239 D. S. Tsvetkov, I. L. Ivanov, D. A. Malyshkin, A. L. Sednev, V. V. Sereda and A. Y. Zuev, *Pure Appl. Chem.*, 2019, **91**, 923–940.
240 S. García-Martín, K. Manabe, E. Urones-Garrote, D. Ávila-Brande, N. Ichikawa and Y. Shimakawa, *Inorg. Chem.*, 2017, **56**, 1412–1417.
241 D. Ávila-Brande, G. King, E. Urones-Garrote, Subakti, A. Llobet and S. García-Martín, *Adv. Funct. Mater.*, 2014, **24**, 2510–2517.
242 A. Maignan, C. Martin, D. Pelloquin, N. Nguyen and B. Raveau, *J. Solid State Chem.*, 1999, **142**, 247–260.

243 D. Garcés, C. F. Setevich, A. Caneiro, G. J. Cuello and L. Mogni, *J. Appl. Crystallogr.*, 2014, **47**, 325–334.
244 T. Nakajima, M. Ichihara and Y. Ueda, *J. Phys. Soc. Jpn.*, 2005, **74**, 1572–1577.
245 E.-L. Rautama, P. Boullay, A. K. Kundu, V. Caignaert, V. Pralong, M. Karppinen and B. Raveau, *Chem. Mater.*, 2008, **20**, 2742–2750.
246 P. Karen, P. M. Woodward, J. Lindén, T. Vogt, A. Studer and P. Fischer, *Phys. Rev. B: Condens. Matter Mater. Phys.*, 2001, **64**, 214405.
247 J. B. Goodenough, *J. Alloys Compd.*, 1997, **262–263**, 1–9.
248 V. A. Cherepanov, T. V. Aksenova, L. Y. Gavrilova and K. N. Mikhaleva, *Solid State Ionics*, 2011, **188**, 53–57.
249 J. Lindén, M. Kochi, K. Lehmus, T. Pietari, M. Karppinen and H. Yamauchi, *J. Solid State Chem.*, 2002, **166**, 118–127.
250 A. I. Klyndyuk, *Phys. Solid State*, 2008, **50**, 609.
251 J. Nakamura, J. Lindén, H. Suematsu, M. Karppinen and H. Yamauchi, *Phys. C Supercond.*, 2000, **338**, 121–125.
252 A. W. Mombru, C. Christides, A. Lappas, K. Prassides, M. Pissas, C. Mitros and D. Niarchos, *Inorg. Chem.*, 1994, **33**, 1255–1258.
253 A. C. Tomkiewicz, M. A. Tamimi, A. Huq and S. McIntosh, *J. Power Sources*, 2016, **330**, 240–245.
254 T. Nakamura, Y. Ling and K. Amezawa, *J. Mater. Chem. A*, 2015, **3**, 10471–10479.
255 V. V. Kharton, M. V. Patrakeev, E. V. Tsipis, M. Avdeev, E. N. Naumovich, P. V. Anikina and J. C. Waerenborgh, *Solid State Ionics*, 2010, **181**, 1052–1063.
256 V. V. Kharton, A. V. Kovalevsky, M. Avdeev, E. V. Tsipis, M. V. Patrakeev, A. A. Yaremchenko, E. N. Naumovich and J. R. Frade, *Chem. Mater.*, 2007, **19**, 2027–2033.
257 T. Nakamura, K. Yashiro, K. Sato and J. Mizusaki, *Solid State Ionics*, 2010, **181**, 292–299.
258 T. Nakamura and K. Amezawa, 2016 IEEE 16th International Conference on Nanotechnology (IEEE-NANO), *Chemically-induced structural deformation of layered perovskite oxides*, 2016, pp. 429–430, DOI: 10.1109/NANO.2016.7751481.
259 T. Nakamura, K. Yashiro, K. Sato and J. Mizusaki, *Solid State Ionics*, 2010, **181**, 402–411.
260 L. V. Mogni, F. D. Prado, G. J. Cuello and A. Caneiro, *Chem. Mater.*, 2009, **21**, 2614–2623.
261 C. Chatzichristodoulou, B. C. Hauback and P. V. Hendriksen, *J. Solid State Chem.*, 2013, **201**, 164–171.
262 C. Chatzichristodoulou, C. Schönbeck, A. Hagen and P. V. Hendriksen, *Solid State Ionics*, 2013, **232**, 68–79.
263 G. Conforto, R. Ruess, D. Schröder, E. Trevisanello, R. Fantin, F. H. Richter and J. Janek, *J. Electrochem. Soc.*, 2021, **168**, 070546.
264 2019.
265 P. Li, Y. Zhao, Y. Shen and S.-H. Bo, *Journal of Physics: Energy*, 2020, **2**, 022002.
266 S. P. S. Badwal, D. Fini, F. T. Ciacchi, C. Munnings, J. A. Kimpton and J. Drennan, *J. Mater. Chem. A*, 2013, **1**, 10768–10782.
267 D. Clerici, F. Mocera and A. Somà, *Energies*, 2021, **14**, 6281.
268 H. Li, N. Zhang, J. Li and J. R. Dahn, *J. Electrochem. Soc.*, 2018, **165**, A2985–A2993.
269 V. Malavé, J. R. Berger and P. A. Martin, *J. Appl. Mech.*, 2014, 81.
270 C. Xu, K. Märker, J. Lee, A. Mahadevegowda, P. J. Reeves, S. J. Day, M. F. Groh, S. P. Emge, C. Ducati, B. Layla Mehdi, C. C. Tang and C. P. Grey, *Nat. Mater.*, 2021, **20**, 84–92.
271 M. T. McDowell, *MRS Bull.*, 2020, **45**, 889–890.
272 W. H. Woodford, W. C. Carter and Y.-M. Chiang, *Energy Environ. Sci.*, 2012, **5**, 8014–8024.
273 B. Koo, K. Kim, J. K. Kim, H. Kwon, J. W. Han and W. Jung, *Joule*, 2018, **2**, 1476–1499.
274 B. Koo, H. Kwon, Y. Kim, H. G. Seo, J. W. Han and W. Jung, *Energy Environ. Sci.*, 2018, **11**, 71–77.
275 E. Mishuk, A. Ushakov, E. Makagon, S. R. Cohen, E. Wachtel, T. Paul, Y. Tsur, V. Y. Shur, A. Kholkin and I. Lubomirsky, *Adv. Mater. Interfac.*, 2019, **6**, 1801592.
276 E. Makagon, E. Wachtel, L. Houben, S. R. Cohen, Y. Li, J. Li, A. I. Frenkel and I. Lubomirsky, *Adv. Funct. Mater.*, 2021, **31**, 2006712.
277 N. Manca, G. Mattoni, M. Pelassa, W. J. Venstra, H. S. J. van der Zant and A. D. Caviglia, *ACS Appl. Mater. Interfaces*, 2019, **11**, 44438–44443.
278 A. A. Bukharaev, A. K. Zvezdin, A. P. Pyatakov and Y. K. Fetisov, *Phys. Usp.*, 2018, **61**, 1175–1212.
279 S. Kim, S. J. Choi, K. Zhao, H. Yang, G. Gobbi, S. Zhang and J. Li, *Nat. Commun.*, 2016, **7**, 10146.
280 Y. M. Gerbshtein, N. E. Timoshchenko, A. D. Muradov and A. Z. Rakhimbekov, *Phys. Solid State*, 1997, **39**, 521–527.
281 J. R. Petrie, H. Jeen, S. C. Barron, T. L. Meyer and H. N. Lee, *J. Am. Chem. Soc.*, 2016, **138**, 7252–7255.
282 U. Aschauer, R. Pfenninger, S. M. Selbach, T. Grande and N. A. Spaldin, *Phys. Rev. B: Condens. Matter Mater. Phys.*, 2013, **88**, 054111.
283 A. Marthinsen, C. Faber, U. Aschauer, N. A. Spaldin and S. M. Selbach, *MRS Commun.*, 2016, **6**, 182–191.
284 R. U. Chandrasena, W. Yang, Q. Lei, M. U. Delgado-Jaime, K. D. Wijesekara, M. Golalikhani, B. A. Davidson, E. Arenholz, K. Kobayashi, M. Kobata, F. M. F. de Groot, U. Aschauer, N. A. Spaldin, X. Xi and A. X. Gray, *Nano Lett.*, 2017, **17**, 794–799.
285 K. Wen, W. Lv and W. He, *J. Mater. Chem. A*, 2015, **3**, 20031–20050.
286 A. N. Morozovska, E. A. Eliseev and S. V. Kalinin, *Appl. Phys. Lett.*, 2010, **96**, 222906.
287 E. Strelcov, S. M. Yang, S. Jesse, N. Balke, R. K. Vasudevan and S. V. Kalinin, *Nanoscale*, 2016, **8**, 13838–13858.
288 S. Kalinin, N. Balke, S. Jesse, A. Tselev, A. Kumar, T. M. Arruda, S. Guo and R. Proksch, *Mater. Today*, 2011, **14**, 548–558.
289 S. Doria, N. Yang, A. Kumar, S. Jesse, A. Tebano, C. Aruta, E. Di Bartolomeo, T. M. Arruda, S. V. Kalinin, S. Licoccia and G. Balestrino, *Appl. Phys. Lett.*, 2013, **103**, 171605.
290 D. O. Alikin, A. V. Ievlev, S. Y. Luchkin, A. P. Turygin, V. Y. Shur, S. V. Kalinin and A. L. Kholkin, *Appl. Phys. Lett.*, 2016, **108**, 113106.
291 A. Kumar, F. Ciucci, A. N. Morozovska, S. V. Kalinin and S. Jesse, *Nat. Chem.*, 2011, **3**, 707–713.